2017•2018

Faculteit Industriële ingenieurswetenschappen

master in de industriële wetenschappen: nucleaire technologie

Masterthesis

Study of parameters influencing the response of HPGe-detectors

PROMOTOR :

Prof. dr. Wouter SCHROEYERS

PROMOTOR :

Dhr. Michel BRUGGEMAN

Dr. Mikael HULT

COPROMOTOR :

Dr. Guillaume LUTTER

ing. Leen VERHEYEN

Stef Geelen

Scriptie ingediend tot het behalen van de graad van master in de industriële wetenschappen: nucleaire technologie, afstudeerrichting nucleaire technieken / medisch nucleaire technieken

De transnationale Universiteit Limburg is een uniek samenwerkingsverband van twee universiteiten in twee landen: de Universiteit Hasselt en Maastricht University.

Universiteit Hasselt | Campus Diepenbeek | Agoralaan Gebouw D | BE-3590 Diepenbeek

Universiteit Hasselt | Campus Hasselt | Martelarenlaan 42 | BE-3500 Hasselt

2017 • 2018

Faculteit Industriële ingenieurswetenschappen

master in de industriële wetenschappen: nucleaire technologie

Masterthesis

Study of parameters influencing the response of HPGe-detectors

PROMOTOR :

Prof. dr. Wouter SCHROEYERS

PROMOTOR :

Dhr. Michel BRUGGEMAN

Dr. Mikael HULT

COPROMOTOR :

Dr. Guillaume LUTTER

ing. Leen VERHEYEN

Stef Geelen

Scriptie ingediend tot het behalen van de graad van master in de industriële wetenschappen: nucleaire technologie, afstudeerrichting nucleaire technieken / medisch nucleaire technieken

UHASSELT KU LEUVEN

Foreword

First of all, I would like to thank all the people of the JRC Geel and SCK•CEN to help me during the period of my Master's thesis.

I also would like to thank my promotors: Dr. Bruggeman Michel, Dr. Hult Mikael and Dr. Schroeyers Wouter for their experience they shared with me and their help in creating this Master's thesis.

And special thanks to Dr. Lutter Guillaume for teaching me the methods and procedures for using EGSnrc in this thesis and also for answering all the questions I had. This thesis would not be possible without his help.

Also, many thanks to ing. Marissens Gerd, Stroh Heiko and ing. Verheyen Leen for giving advice and helping me were they could during my thesis.

Last but not least I also would like to thank my parents for this opportunity.

Table of contents

List of tables

List of figures

Abstract

The SCK•CEN, the JRC Geel and the University of Hasselt make use of High Purity Germanium detectors (HPGe) for gamma-ray spectrometry. These detectors have a superior resolution compared to other gamma-ray detectors. However, these detectors still need many corrections for quantitative analysis of radioactivity, nuclide identification or the characterisation of unknown samples. Anno 2018 those corrections are mostly calculated by advanced algorithms involving Monte Carlo simulations. Such simulations require a detailed digital model of the detector. In this thesis EGSnrc software was used to make these simulations. Three topics were investigated. First, the creation of a model for the detector of UHasselt was done. This resulted in an irregular deadlayer with a crater in the middle. Second, a new model for detector T7 was created with the aim to investigate the influence of the parameters in the model. All parameters were changed separately and their individual influence was measured by comparing the relative difference in counting efficiency compared to experimental data. Third, a comparison of two deadlayer thickness calculation methods was done. A first method was based on a method described by Budjas et al. [1] and the second method is based on the differences in attenuation coefficients. The results of this comparison showed that both methods gave a good indication of the deadlayer thickness given that a non-collimated point source of ^{241}Am is used.

Abstract (Nederlands)

Het SCK•CEN, het JRC Geel en de Universiteit van Hasselt maken gebruik van High Purity Germanium detectors (HPGe) voor gammaspectrometrie. Deze detectors hebben een superieure resolutie in vergelijking met andere gamma-ray detectors, maar deze detectors hebben nog veel correcties nodig voor kwantitatieve analyses van radioactiviteit, identificatie van nuclides of karakterisering van onbekende stalen. Anno 2018 worden deze correcties meestal berekend met behulp van geavanceerde algoritmes die gebruik maken van Monte Carlo simulaties. Deze simulaties vereisen een gedetailleerd digitaal model van de detector. In deze thesis werd EGSnrc software gebruikt om deze simulaties uit te voeren. Hierbij werden drie onderwerpen onderzocht. Ten eerste, een model voor de detector van UHasselt werd gemaakt. Ten tweede, een nieuw model voor detector T7 werd gemaakt met de focus op de invloed van de verschillende parameters van het model. Alle parameters werden apart aangepast en hun individuele invloed werd gemeten door het relatieve verschil in efficiëntie te vergelijken. Ten derde, twee methodes om de dikte van de dode laag te berekenen werden vergeleken. De eerste methode was gebaseerd op de methode in Budjas et al. [1] en de tweede methode is gebaseerd op het verschil in attenuatie coëfficiënten. De resultaten gaven aan dat beide methodes een goed indicatie van de dikte van de dode laag geven, maar in elk geval zou een energie kalibratie moeten uitgevoerd worden zodat de dode laag die het beste met de meting overeenkomt wordt gebruikt.

1 Introduction

The Belgian Nuclear Research Centre (SCK•CEN) is one of the biggest research centres in Belgium and researches peaceful applications of radioactivity since 1952. The SCK•CEN is located in Mol, Belgium and works on three major research topics: the safety of nuclear installations; the well-considered management of radioactive waste; human and environmental protection against ionising radiation. One of the installations that can be found at the SCK•CEN is the BR1 reactor or Belgian Reactor 1. This is a graphite moderated air-cooled reactor with natural uranium as fuel. BR1 was built in 1956 making it the oldest reactor of Belgium. A recent research project at the SCK•CEN is MYRRHA, Multipurpose hYbrid Research Reactor for High-tech Applications. This is a reactor that works with an accelerator driven system what makes it one of a kind. Because it is driven by an accelerator the reactor is easier to control and safer than other reactors. Besides reactors the SCK•CEN also searches new and innovative ways for the disposal of radioactive waste and technologies to aid medical science. At the SCK•CEN gamma spectrometry is used to measure volume sources, element concentration and to carry out neutron activation analysis. Therefor the SCK•CEN has multiple High Purity Germanium detectors available with an excellent resolution [2], [3].

The European Commission's Joint Research Centre was established in the EURATOM Treaty, which was signed in Rome 1957. A Central Bureau for Nuclear Measurements (CBNM) was built in Geel as stipulated in Article 8. The core activities involved radionuclide metrology, mass spectrometry and neutron physics. Due to a vast denuclearization campaign, CBNM changed its name to Institute for Reference Materials and Measurements (IRMM) in 1993, which better reflected the core activities. In 2016 the name changed again, this time to JRC-Geel to better promote the corporate identity of the JRC, which has staff at six different sites in Europe. The RadioNuclide Metrology Sector (RN-Sector) of JRC-Geel was the first operational entity of CBNM in 1959. Its main tasks were linked to the realization of the unit Bq for "all" radionuclides (every radionuclide decays in a different way and requires therefore special instrumentation) through primary standardization (i.e. to measure activity without having to rely on a calibration standard. A very important spin-off was to measure accurate decay data. Such activities are still very important but in addition, the RN-Sector, supports all European laboratories that monitor radioactivity in the environment by providing reference materials and proficiency tests. In addition, an underground laboratory has been established in the underground facility HADES which is operated by Euridice at the premises of SCK•CEN in Mol, Belgium. In HADES it is possible to measure gamma-emitters with a background that is 10 000 times lower compared to above ground. This is important for characterizing reference materials and to provide special decay data. Furthermore, the HADES facility is available for European users through the open access program, EUFRAT (European facility for nuclear reaction and decay data measurements). Here applications like environmental tracer studies and studies of natural archives like ice cores and coral can be performed. All detectors in HADES are of the germanium-type. This is nowadays the workhorse of every radiometric laboratory. Also in the above ground laboratories these detectors form the core. It is very important to try to better understand the response of such detectors, which is also part of the work program of the RN-Sector.

At the University of Hasselt HPGe detectors are mainly used for educational and research purposes in the Master of Science in nuclear technology and also the master of science in environmental science. The master of science in nuclear technology is divided in two subdivisions, reactor technology and medical-nuclear techniques. The HPGe detectors of the University of Hasselt are not constantly kept cold what could influence their technical properties. This was also one of the reasons to initiate this Master's thesis.

Together with the institutes mentioned above this Master's thesis was initiated to get a better understanding of the influence of the different parameters of HPGe-detectors. This will be done with Monte Carlo simulations done with EGSnrc software.

2 Literature study

2.1 Working principles

A germanium crystal is a semiconductor, when made into a detector it works like a diode. To understand the underlying mechanism, it is first needed to elaborate on semiconductors. Figure 1 shows that there are three types of solids that can be divided by their kind of electronic structure: insulators, conductors and semiconductors. The band structure of a solid is as follows: there are two bands divided by a so-called band gap. The band gap represents the energy an electron needs or releases when it jumps between these two bands and is also known as the forbidden region. The first band is the valence band. This is the band in which the electrons hold energy and where chemical reactions occur. The second band is the conduction band. In this band the electrons are mobile and can move throughout the crystal. The bandgap is in a direct relation to the resolution of the detector. It determines the lowest energy that an electron needs to cross the bandgap and give a signal.

For insulators the band gap, E_g, is approximately 10 eV, significantly more than the energy surmounted by thermal excitation. It is unfortunately also too high to get a decent resolution for gamma-ray detection [4], [5].

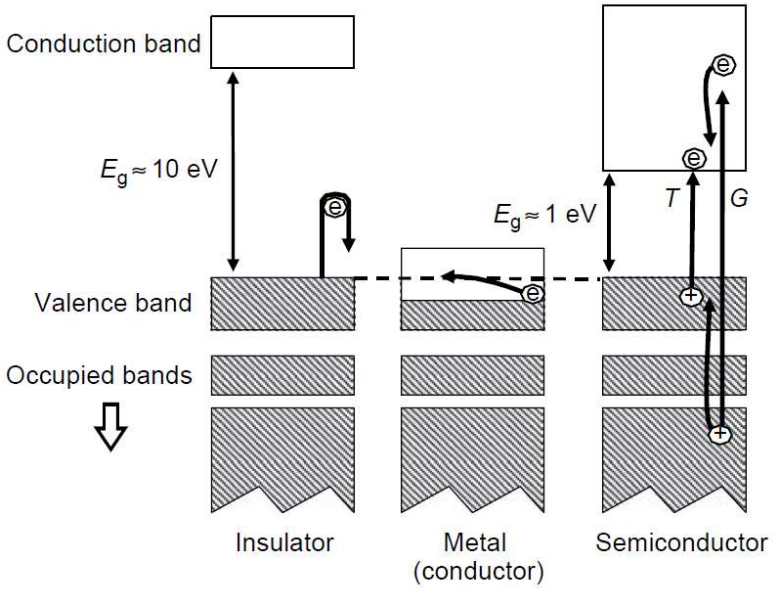

Figure 1: schematic representation of the different electronic structures of insulators, conductors and semiconductors [4, p. 40]

For conductors the band gap is zero. The valence and conduction band merge together what leads to conduction of electrons. For gamma-ray detection this is a bad characteristic because even thermal excitation can trigger a signal. This would make the received signal very noisy and even not readable because the gamma peaks would be in most cases indistinguishable from the noise.

The last option are semiconductors. Here there is an approximate band gap, E_g, of 1 eV. This energy is low enough for a good resolution but it is also low enough for thermal excitations. Under normal conditions there will still be a small population of electrons in the conduction band because of thermal excitations. These electrons cause a constant leakage current and a noisy signal. The solution for these thermal excitations is to cool the crystal down what is mostly done with liquid nitrogen with a temperature of 77 K. This is not the case for all semiconductors but only when the bandgap of the semiconductor is lower than the thermal excitation energy. The probability of an electron being

promoted to the conduction band is shown in equation 1 and is strongly dependent on the temperature T, k stands for the Boltzmann constant and E_g for the band gap [4], [6].

$$p(T) \propto T^{3/2} e^{-E_g/2k} \qquad (1, [4])$$

To let the electron and holes move, a high voltage must be applied over the crystal. To apply the high voltage a cathode and anode are required. The cathode is created by lithium interstitial diffusion. The crystal is heated to a few hundred degrees Celsius and lowered into a bath of lithium what leads to diffusion of lithium into the crystal to create a cathode or n+ contact. The anode or p+ contact is created differently. Here boron is implanted by use of an ion gun. The result of the different creation processes is a thicker deadlayer for the lithium diffused cathode. A deadlayer is a part of the crystal where interaction with the crystal does not result in a signal. This deadlayer is the direct consequence of the creation of the electrodes. Another issue that rises is that the lithium keeps diffusing and even more when the crystal is brought back to room temperature [7]. This causes the deadlayer to grow what has a negative influence on the crystals detection efficiency [4], [6].

When both sides are doped a depletion region emerges. Here electrons and holes recombine. This is also the region that allows gamma-rays to interact with the crystal and create electron-hole pairs for the creation of an electrical pulse. However, without bias the depletion region will be too thin to really give a pulse create a detector. Therefore, a reversed biased junction is made. A reversed biased junction is made by putting a positive voltage on the negative type semiconductor. Because a positive charge is placed on the cathode and a negative charge on the anode the depletion region will increase, the thickness of the depletion region can be estimated by equation 2 [4], [6].

$$d = [2\kappa\mu\rho(V_0 + V_b)]^{1/2} \qquad (2, [4])$$

In the equation, d is the thickness of the depletion region, V_0 and V_b are the contact and bias voltages, κ is the dielectric constant, ρ is the resistivity of the material and μ is the mobility of the majority charge carrier in the material. The majority charge is dependent of the type of semiconductor, with p-type semiconductors this are the holes and with n-type semiconductors this are the electrons. What type of semiconductor is used depends on the choice of the manufacturer and the purpose of the detector [4]. The differences between these two types are explained in the chapter p- and n-type detectors.

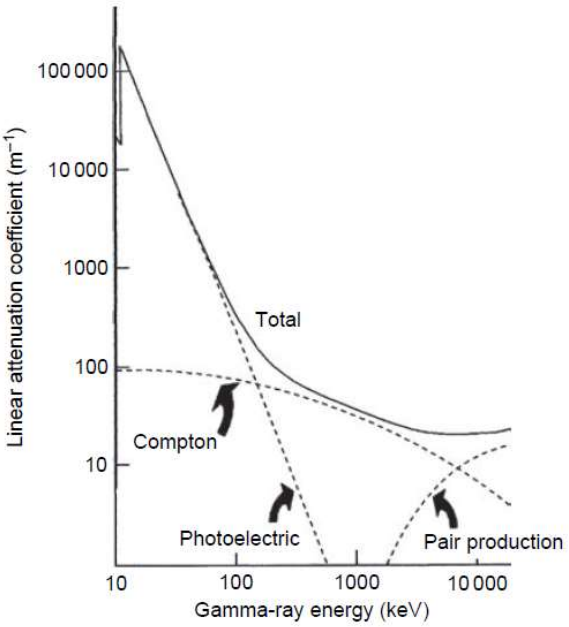

Figure 2: Attenuation coefficient of germanium per energy and per type of interaction [4, p. 26]

When a gamma-ray interacts with the germanium crystal it will excite electrons with energies far beyond the energies obtained with thermal excitation. The possible interactions are the photo-electric effect, Compton scattering and pair production as can be seen in Figure 2. The higher energy causes that not only electrons of the valance band are promoted but also electrons from bands beneath it. The excitations let the electrons jump to the conduction band what creates electron-hole pairs. The number of created pairs, n depends on the absorbed energy E_{abs} and the average energy needed to create one electron-hole pair ε as shown in equation 3. These pairs will migrate to the proper electrode as a result of the reversed bias voltage. The movement of the pairs together with their charge creates an electrical pulse. This pulse needs to be amplified to be registered by a multichannel analyser [4]–[6].

$$n = \frac{E_{abs}}{\varepsilon} \qquad (3, [4])$$

The way electrons and holes move towards respectively the anode and cathode is as follows. Firstly, in the presence of an external electrical field an electron jumps to a vacancy or hole, by doing this the hole disappears and the electron has moved towards the anode. Another thing that happens in that action is that by jumping to a hole the electron has created a new hole that appears to go to the cathode, this movement is shown in Figure 3. Because both, electrons and holes, carry charge with them they create an electrical current. Table 1 gives different characteristics for different gamma ray detectors, one point of notice is that the mobility of electrons and holes is not the same. The difference between silicon and germanium detectors is clearly visible in Table 1 and Figure 4. In Figure 4 the superior resolution of germanium detectors is visible over the total energy range depicted. However, germanium detectors should be cooled constantly to keep their superior resolution, this is not the case for silicon detectors what makes them easier in use [4], [6].

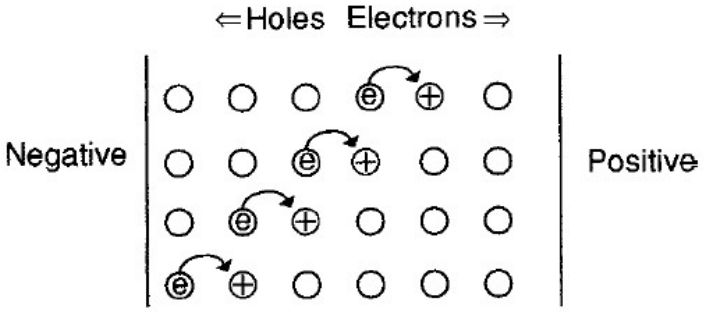

Figure 3: Schematic drawing of the movement of holes and electrons through the germanium crystal [4, p. 40]

Table 1:Data about different gamma-ray detectors [4, p. 41]

Material	Atomic number	Operating temperature	Band gap (eV)[a]	ε (eV)[a,b]	Density ($g\,cm^{-3}$)	Mobility($cm^2\ V^{-1}\ s^{-1}$)[a]	
						Electrons	Holes
Si	14	RT	1.106	3.62	2.33	1350	480
Ge	32	Liquid N_2 (77 K)	0.67	2.96	5.32	3.6×10^4	4.2×10^4
CdTe	48, 52	RT	1.47	4.43	6.06	1000	80
CdZnTe	48, 30, 52	RT	1.57	4.64	5.78	1000	50–80
HgI_2	80, 53	RT	2.13	4.22	6.30	100	4
GaAs	31, 33	RT	1.45	4.51	5.35	8000	400
TlBr	81, 35	−20 °C	2.68	?	7.56	—	—
PbI_2	82, 53	—	2.6	7.68	6.16	8	2
GaSe	31, 34	—	2.03	6.3	4.55	—	—
AlSb	13, 51	—	1.62	5.05	4.26	—	—
CdSe	48, 34	—	1.75	?	5.74	—	—

[a] Values are given at 77 K for Ge and 300 K otherwise.
[b] Electron–hole creation energy.

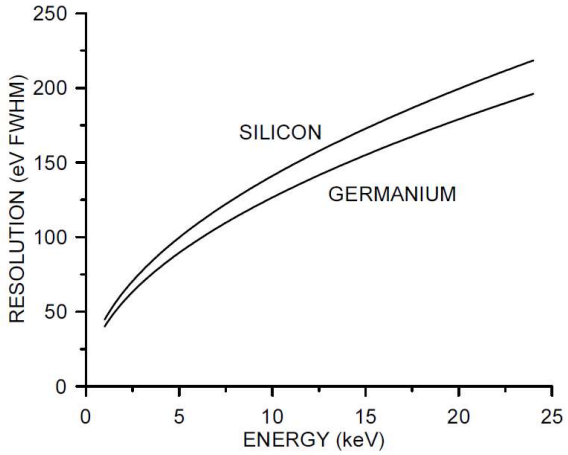

Figure 4: Resolution in eV full width half maximum in function of the energy displayed for Si and Ge [5, p. 54]

2.2 Type of detector

2.2.1 Geometry

The placement and geometry of all the involved parts play a role in the absolute efficiency of the detector-source configuration. The shape of the detector is one of the most important parameters and can be divided into three categories: planar, coaxial and well. Each of these configurations has its advantages and problems. In

Figure 5 and Figure 6 these geometries are displayed.

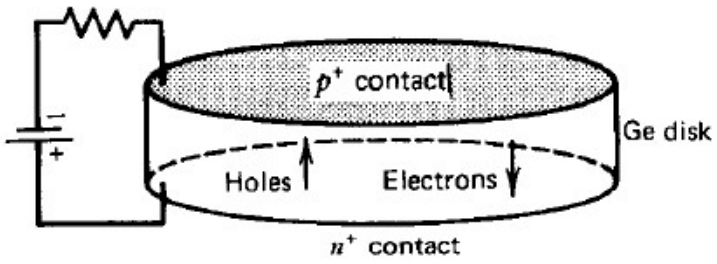

Figure 5: Schematic drawing of a planar HPGe detector [6, p. 407]

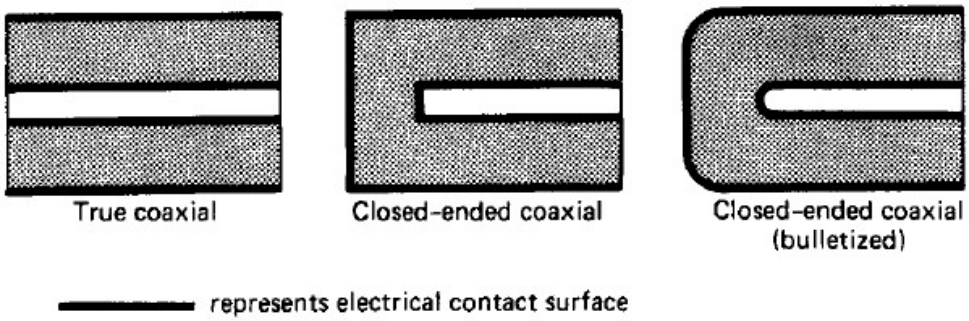

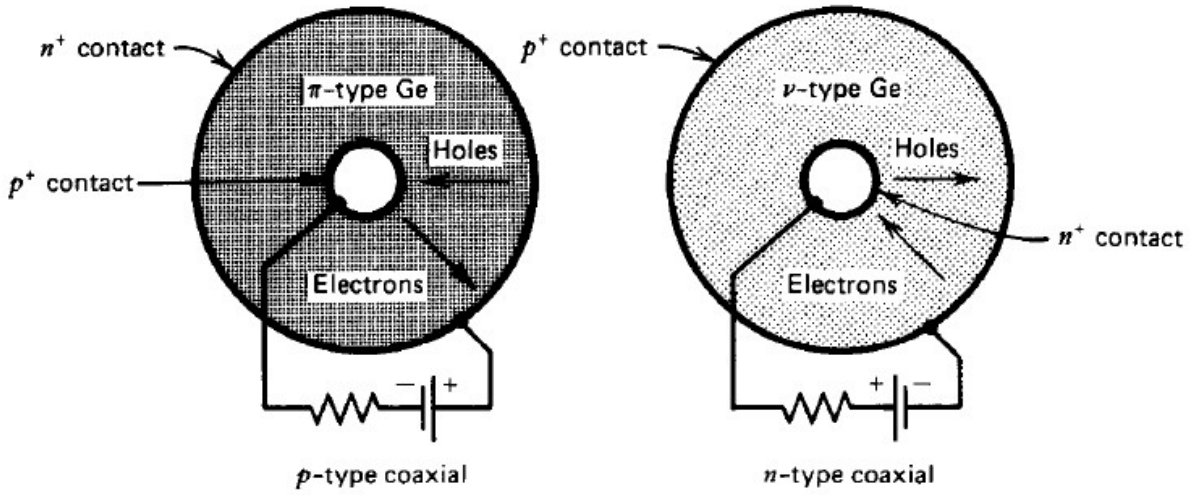

Figure 6: Schematic axial drawing of a coaxial HPGe detector (up) together with a schematic of the diode characteristics (down) [6, p. 409]

The planar geometry has two parallel electrodes that are a n+ and a p+ contact. The high purity germanium crystal in between these electrodes is only a few centimetres in diameter and less than 2 cm in height. This is necessary because the depletion region will only reach that distance. This gives the problem that the active volume is relatively small compared to the other geometries and thus only useable for low energy gamma- and X-rays. The main advantage with a planar geometry is that the applied electrical field is almost completely uniform what results in a constant electron and hole drift, with the coaxial geometry the electrical field is radial and not uniform [4], [6], [8].

With a true coaxial geometry, the core of the cylindrical high purity germanium crystal is removed. Then the first electrode is created on the outer cylindrical surface and the second on the inner cylindrical surface where the core was supposed to be. Because the crystals can be made longer in the axial direction, larger active volumes can be achieved. Another advantage is that by using a small inner diameter, large-volume detectors with a lower capacitance can be created than would be possible with a planar geometry. This is positive because a smaller capacitance creates a better resolution. In equation 4 and 5 the capacitance is calculated [4], [6].

$$C_{planar} = \kappa A/(4\pi d) \qquad \text{(4, [4])}$$

$$C_{coaxial} = \kappa h/(2\ln(r_2/r_1) \qquad \text{(5, [4])}$$

In these equations κ stands for the dielectric constant for germanium, A is the surface of the planar detector, d is the thickness of the planar detector, h is the height of the coaxial detector and r_1 and r_2 are respectively the inner and outer radius of the detector. The electrical field lines are radial, if this was not the case there will be regions of lower electrical field strength what has a negative influence on the mobility of the electron-hole pairs. However, since the field is radial it is not uniformly distributed what leads to a different kind of motion for the electron-hole pairs [4], [6].

A closed-ended coaxial geometry is comparable with a true coaxial geometry with the difference that the core is not fully removed from the crystal. Instead a so-called bore hole is drilled into one of the parallel surfaces from the cylindrical high purity germanium crystal. A first problem that arises is that on the closed end of the crystal the electrical field is no longer radial and there is a tendency to have lower field strengths in the corners of the crystal. As mentioned before this has a negative influence on the mobility of the electron-hole pairs. To reduce the difference in electrical field strength, bulletization is used. Bulletization is the rounding of the corners of the crystal and bore hole to eliminate the low field strength regions. Figure 7 shows a schematic drawing of a closed-ended coaxial HPGe-detector [4], [6], [9].

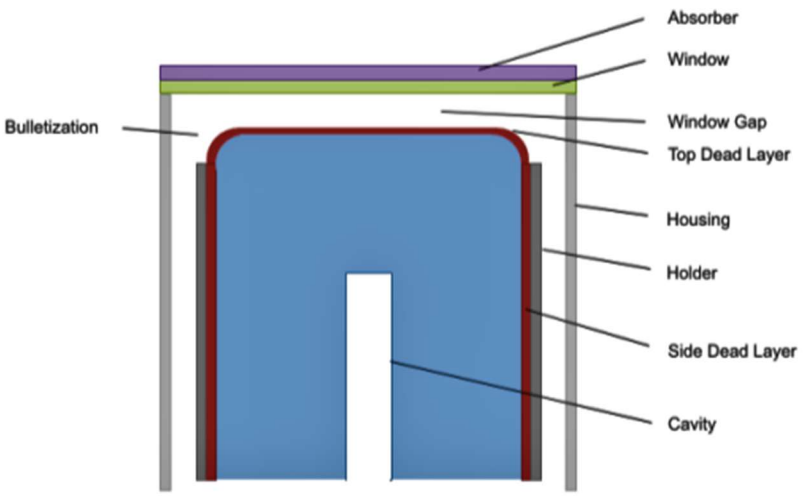

Figure 7: Drawing of a standard close-ended coaxial HPGe detector

The last geometry is the well geometry. The well geometry works the same way as the closed end coaxial geometry and the main advantage is its large coverage of the source that is placed inside the well. Because of the large coverage a well detector has an excellent detection efficiency compared to the planar and coaxial detectors [4], [6].

Other things that are linked to the geometry of the detector source setup are tilting of the crystal, bulletization and the homogeneity and placement of the source. The last factor is especially important when using Monte Carlo models because of the inverse-square law. The influence of a tilted crystal and bulletization are explained in [9]. It states that realistic tilting of the crystal, to a maximum of 5°, has no significant influence on the efficiency but the absence of bulletization in the Monte Carlo model has a significant influence on the efficiency for low energies. It caused an overestimation of the efficiency of several percent. However, for higher energies the influence was less significant. The homogeneity of the source in the Monte Carlo model could differ from the one in reality. This could also lead to a wrongly calculated efficiency. A different placement of the source as in the model also leads to a wrongly calculated efficiency [4], [10], [11].

Something that is indirectly linked to the geometry is microphonic noise. This type of noise is a consequence of vibrations that alter the geometry of different components of the mount and the detector what causes a change in the capacitance resulting in noise.

2.2.2 p- and n-type detector

The main differences between the p- and n-type coaxial detectors are the deadlayer thickness and the kind of impurities in the crystal. As mentioned before, the impurities for p-type detectors are holes and for n-type detectors electrons. The outer deadlayer of the p-type coaxial detector is relatively large compared to the outer deadlayer of the n-type coaxial detector. This distinction is clearly visible in the difference in intrinsic efficiency in Figure 8. As shown in Fig. 2, below 100 keV, photoelectric absorption is the dominant interaction, which leads to a maximum for both detector types. However, the efficiency of the p-type coaxial detector with energies below 100 keV is significantly lower compared to the n-type coaxial detector. The cause of that difference is the larger deadlayer that attenuates most of the low energy gamma-rays. With the n-type coaxial detector the efficiency for lower energies remains more constant from 100 keV on. However, there is a small notch at 11 keV. The notch is caused by the K-shell binding energy of Ge. The K-shell absorption only requires a small depth and because there is first a deadlayer there will be a significant amount of lost counts. With lower energies the K-shell binding energy is no longer available what results in a sudden rise. Hereafter, the efficiency starts to decrease because of the thin deadlayer. For higher energies both the n- and p-type coaxial detector follow a similar curve. In the energy range from 100 keV to 1 MeV the gamma-rays still

interact with the detector but Compton scattering is among the interactions. A photon from Compton scattering has a relatively high probability to escape the detector, what lowers the efficiency. Above 1 MeV a significant fraction of the gamma-rays just passes through the crystal without any interaction [4], [6].

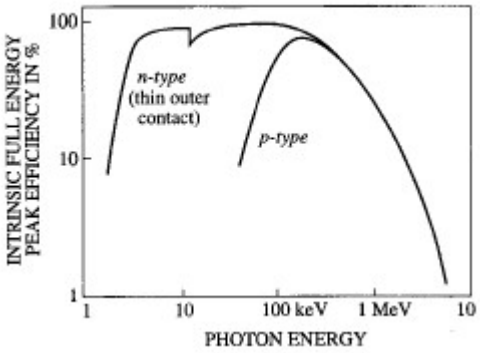

Figure 8: Normal intrinsic FEP efficiency calibration for n- and p-type HPGe detectors [6, p. 444]

2.3 Acquiring results

To use a HPGe detector for activity measurements or gamma-ray analysis it is important to have an estimation of the energy efficiency of the detector. The full energy peak (FEP) detection efficiency, ε, is the most difficult to determine because it depends on multiple parameters. In equation 6 these parameters are given in relation to the activity A. Herein, C is the number of counts that is measured or the total surface below the peak without the continuum and background, P_γ is the emission probability of the gamma-ray, t_l is the live counting time of the measurement, λ is the decay constant of the nuclide, t_d is the time that passed relative to the reference time and t_r is the real measuring time.

$$A = \frac{C}{\varepsilon \times P_\gamma \times t_l} \times e^{\lambda \times t_d} \times \frac{\lambda \times t_r}{1 - e^{-\lambda \times t_r}} \qquad (6)$$

2.3.1 Peak analysis

The peak analysis was done with GENIE 2000. The Canberra GENIE 2000 software is a spectroscopy acquisition and analysis software developed by Canberra industries (now under Mirion Technologies). It was used to acquire data for all the measurements and also for fitting peaks to the spectra.

If an uncooled HPGe detector is used there will be a significant thermal leakage current. This is due to the thermal excitations of electrons that make them able to jump over the 0.7 eV band gap. Because of the numerous electrons that are located at the conduction band, a leakage current emerges. Another source of leakage current are surface impurities that cause surface leakage currents. A last source of leakage current is due to impurities that are created by radiation damage. Leakage currents, that are mainly in the region of pA, have several undesirable effects: the integrated current over typical signal processing times can exceed the signal; noise on the signal is created what has a negative effect on the energy resolution; the power dissipation in the detector increases. The last effect increases the temperature what gives rise to even more leakage current. This is why cooling the HPGe detector is necessary [4]–[6], [12]–[14].

2.3.2 Deadlayer

The first and most difficult parameter to determine is the deadlayer, especially with low energy gamma-rays. As explained earlier, a HPGe-detector is essentially a diode in which one tries to maximize the depletion region. The deadlayers are situated at the p+ and n+ contacts of the germanium crystal and absorbs a part of the gamma-rays. These gamma-rays do not contribute to the electrical signal what means that there is a loss of counts and corrections must be made. However, different studies

suggest that there are signals that originate from the deadlayer. This is possible if the signals originate from the transition region where the deadlayer becomes the active crystal [7], [15], [16].
The biggest problem with the deadlayer is that it cannot be measured directly. For the boron implanted anode it can be calculated with the data of the ion gun, but for the lithium diffused cathode it is impossible because there is not enough data on the diffusion constants of lithium in germanium crystals at room temperature and below. The lithium also diffuses further when the crystal is at room temperature what adds another uncertainty [4], [6], [7], [16]. Because of these uncertainties a different approach is needed.

2.3.3 True coincidence summing

To explain True coincidence summing or cascade summing some terms should be defined first:

- Live time: the time when the detector is not processing a pulse and can receive another one it is the effective counting period of the system.
- Dead time: the time that is used to process the received signal by the electronics and the detector and herein no pulses can be obtained. The dead time is a combination of the resolving time and the response time.
- Resolving time: the time the electronics need for processing the signals
- Response time: the time the detector needs to give a signal.
- Gamma-ray cascade: some radionuclides with a complex decay scheme that may have several gamma-rays being emitted after each other in a cascade.

The time in between the two (or more) gamma-rays is so short that they appear to be created simultaneous. If the time between the detection of two gamma-rays is shorter than the resolving time of the detection system, the energy of the two gamma-rays will be added to each other and create a single pulse, what is the definition true coincidence summing. The result is that there will be loss of counts and loss of efficiency at the full energy peak of each individual gamma-ray. The created summing peak is also Gaussian what means that pulse rejection will not be effective [4], [6], [17].

To solve this it is necessary to reduce the probability that two simultaneously created gamma-rays are also simultaneously detected. This probability is dependent on the solid angle subtended by the source and the detector. The solid angle is the probability that one gamma-ray coming from the source will be incident on the detector and can be expressed in either steradians or percentages (by dividing the steradians by 4π). Figure 9 shows an example of how the probability can be lowered, in this case the source that is placed at 115 mm from the detector's endcap will have a negligible probability on true coincidence summing so it can be ignored. For the source that is placed on the endcap this is not the case. To calculate the according probability, P, equation 6,7 and 8 were used.

$$P = (R - D)^2/(2R)^2 \qquad (6, [4])$$

$$D = d + d_0 \qquad (7, [4])$$

$$R = \sqrt{r^2 + D^2} \qquad (8, [4])$$

Herein R stands for the radius of the sphere into which the source emits, d is the source to endcap distance, d_0 is the endcap to crystal distance and r stands for the detector radius. This shows that for large detectors the true coincidence summing effect has a more significant influence [18]. True coincidence summing in a spectrum can be recognized by noticing a sum coincidence peak that does not belong there in a normal spectrum and is placed at the sum of the energies of two other peaks [4], [6], [17], [19]. Coincidence summing depends on the nuclide and the geometry of the setup, it does not depend on the activity of the sample or source.

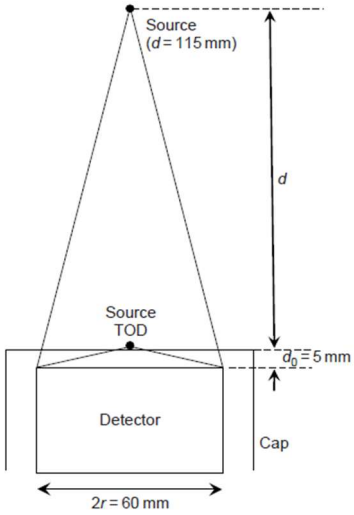

Figure 9: Geometrical arrangements of two different setups with focus on the solid angle [4, p. 166]

2.3.4 Pile-up/ random summing

Random summing or pile-up occurs mostly when the source has a high count rate and the simultaneous detection of two or more gamma-rays that are not related to each other occurs e.g. originating from different disintegrations. The probability of pile-up grows with the square root of the count rate and also with the crystal's volume [20]. Interference with the surrounding matter is also a factor that must be accounted for. The explanation is the same as with true coincidence summing. The difference between random and true coincidence summing is that random summing is linked to the activity of the source, while cascade summing is linked to the position of the source. A second difference is present in the pulse shape. The output pulse shape with true coincidence summing is like a Gaussian distribution while with random summing the pulse will be a mixture of two or more overlapping pulses. Because of this shift it is possible to reject these pulses by means of pile-up rejection. The random summing results in loss of counts and loss of efficiency, as was the case with true coincidence summing [4], [5], [21].

2.4 Detection efficiency

The most significant parameter in gamma spectrometry is the full energy peak efficiency (FEP efficiency or ε). Absolute FEP efficiency is the ratio of the number of counts detected in a peak to the number emitted by the source. This definition is given in symbols in equation 9 [4], [10], [22].

$$\varepsilon = R/(S \times P_\gamma) \qquad (9, [4])$$

Herein R stands for the full-energy peak count rate in counts per second, S is the source strength in disintegrations per second and P_γ is the probability of emission of that particular gamma-ray that is being measured [4], [10], [22].

It is best to keep in mind that the source strength will change over time and that the source to detector geometry plays an important role in the absolute FEP efficiency calibration since the inverse quadratic law applies here. The geometry is also important when the used source is volumetric, equation 9 should therefore only be used with point sources [11], [23]. With an absolute FEP efficiency calibration the FEP efficiency of different energies is calculated and plotted on a graph. Intrinsic FEP efficiency is different from the absolute FEP efficiency because it is not dependent on the source to detector geometry because it only looks at the ratio between the number of particles entering the detector and the number of particles that are detected. A normal intrinsic FEP efficiency calibration for n- and p-type coaxial HPGe detectors looks like the one displayed in Figure 8 [4].

2.5 Monte Carlo code and simulations

Monte Carlo simulations allow us to perform probabilistic events in higher numbers to be statistically relevant. To do this, it uses a pseudo random number generator. The acquired random numbers are assigned to different parameters that affect the particles. First, a simulation file should be formed. The simulation file holds all the information of the geometry, material, particles and more. Second, histories or events have to be initiated. This is the creation of the particles and their progeny created by interaction with the surrounding material. With HPGe detectors, particles that interact with the crystal are the most interesting. By adjusting the geometry or material in the simulation file it is possible to adapt the characteristics of the crystal to look for the impact of these changes.

2.5.1 Iterative process

To obtain a representative computer model a multiple step iterative process has to be followed. In Figure 10 such a process is shown. The adaptation of a parameter happens based on the difference between the FEP efficiency of the measurement and the simulation. The parameters that are changed are the endcap to crystal distance, the side deadlayer thickness and the deadlayer thickness. This is further explained in the chapter of detector T7.

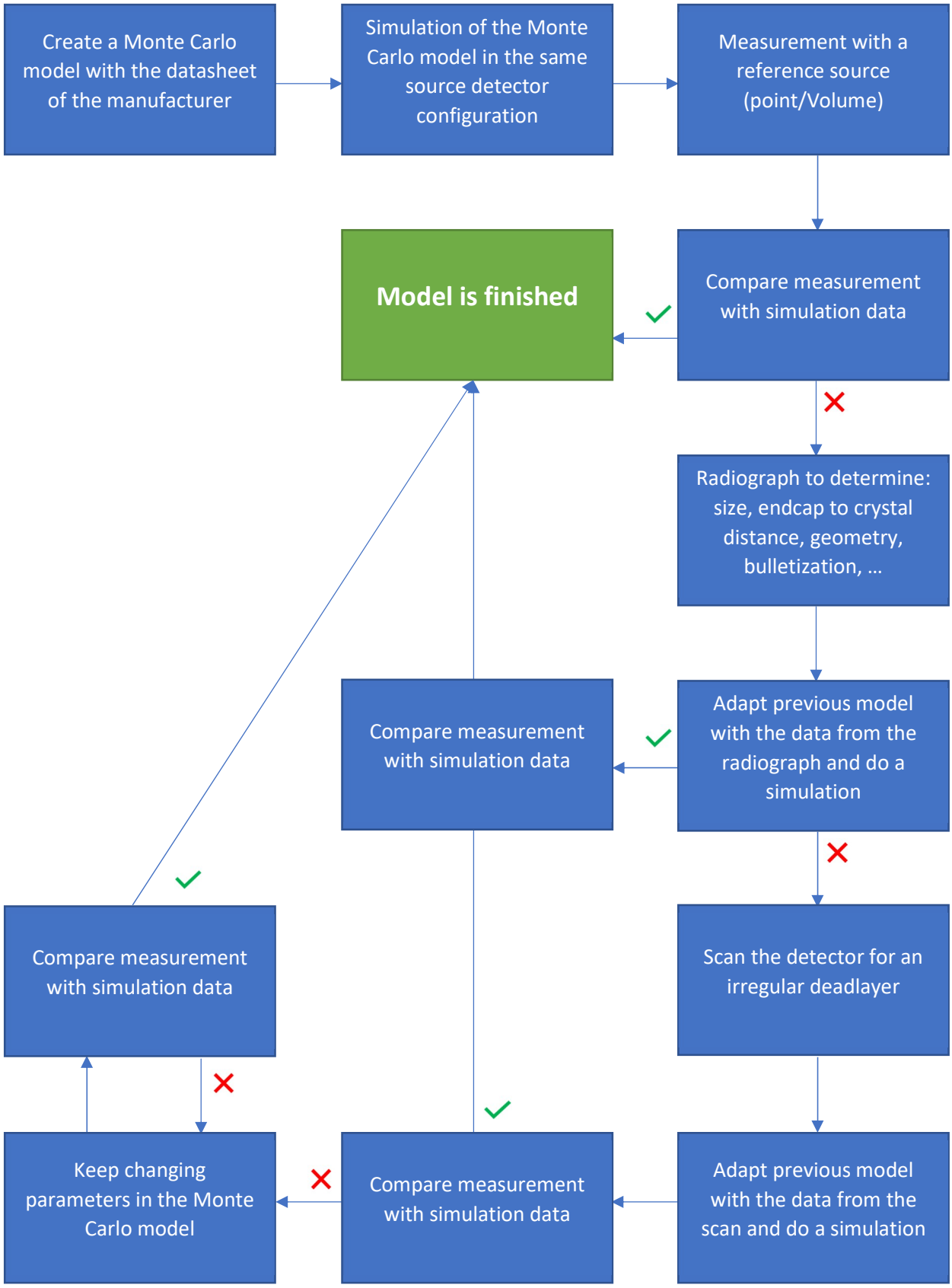

Figure 10: Flowchart for the iterative process of creating a model

3 Methods and Materials

To create the model of a HPGe detector it is important to have an estimation of the deadlayer thickness.

3.1 Methods for deadlayer thickness calculation

The deadlayer thickness can be theoretically obtained by two methods. The first one is explained in Budjas et al. [1] and the second one is obtained from Dr. M. Bruggeman. The method of Budjas et al. works on the principle that the efficiency of experimental measurements should agree with the efficiencies obtained by the model and gives the averaged deadlayer over the top surface of the crystal. To make this method less dependent on the source Budjas et al. [1] chose to use the relative counting efficiency being the ratio between the sum of the 99 and 103 keV counting efficiencies divided by the efficiency of the 59 keV line of an ^{241}Am source. The sum of the 99 and 103 keV lines was taken because the separation between the two gamma lines was comparable to the energy resolution of the detector that was used in their work. Hereafter several detector models have to be investigated each with a different deadlayer thickness. These models have to be simulated with the same energies as the real measurement to create an efficiency to deadlayer thickness curve as shown in Figure 11 [1].

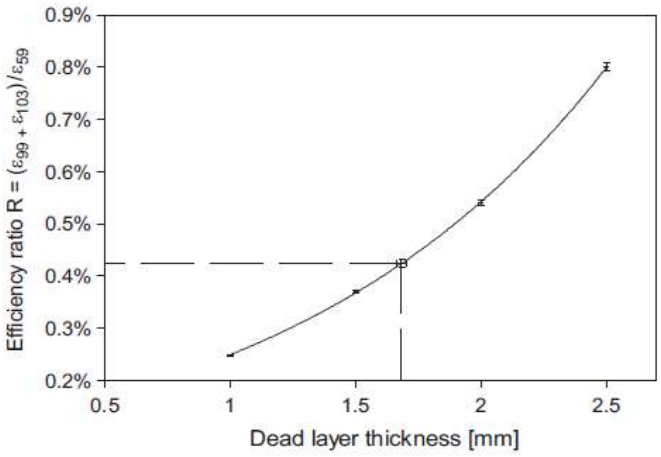

Figure 11: Efficiency ratio in function of the deadlayer thickness [1, p. 3]

In this curve the actual relative efficiency obtained in the measurement is then used to obtain the corresponding deadlayer value (see Figure 11). Three things are important with Budjas' method. First, the source cannot be collimated, because the method only works by averaging the deadlayer over the total top surface. Second, the source should be positioned at more than 10 cm to make sure that coincidence summing is kept at a minimum and that the angle of the incident gamma-rays is not too large. Hence, this would cause them to cross the deadlayer diagonal what gives the impression of a thicker deadlayer. Last, if the detector has an energy resolution that allows a clear distinction between the 99 and the 103 keV lines, the two gamma-rays should still be taken together if the efficiency difference between the two gamma-rays is negligible. Using both peaks improves the uncertainty on the counts and if there is an overlap it will reduce the error on the peak fitting of the two gamma-rays.

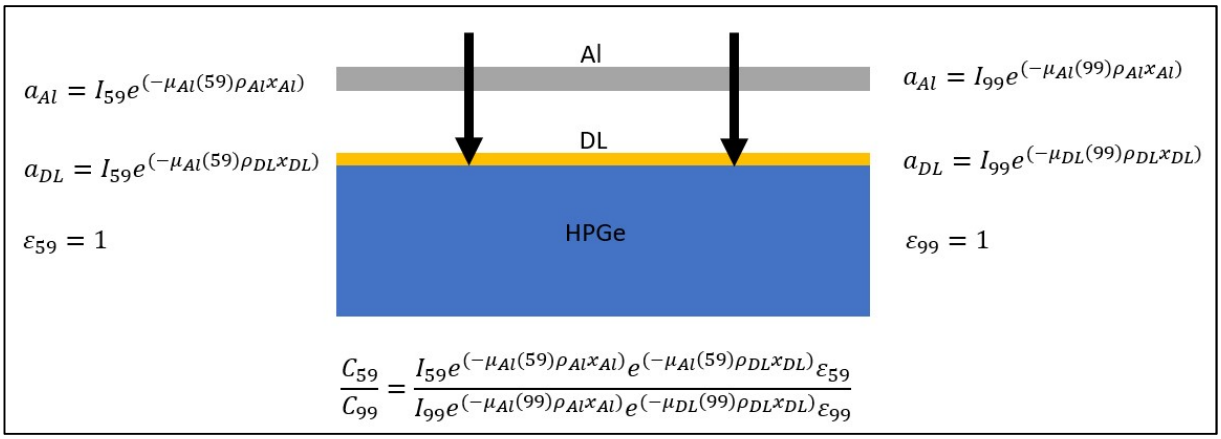

Figure 12: Visualisation of the method based on attenuation coefficients

The method proposed by Dr. Bruggeman relies on another aspect of the deadlayer and is illustrated in Figure 12. Here the attenuation of two different gamma-ray energies is compared. The main problem with this method is that reliable attenuation coefficients are needed. An assumption that must be made is that neither of the gamma-rays escapes the detector crystal, what results in a geometrical efficiency of 1. Every attenuation factor has to be combined into one equation. Hereafter, the equation has to be reformed to be in function of the deadlayer thickness x_{DL}. The equation that comes forth by doing this is given below.

$$x_{DL} = \frac{\ln\left(\frac{C_{59}I_{99}e^{\left(-\mu_{Al}(99)\rho_{Al}x_{Al}\right)}\varepsilon_{99}}{C_{99}I_{59}e^{\left(-\mu_{Al}(59)\rho_{Al}x_{Al}\right)}\varepsilon_{59}}\right)}{(\mu_{DL}(99)-\mu_{DL}(59))\rho_{DL}} \qquad (10)$$

Herein C stands for the number of counts, μ is the attenuation coefficient, ρ is the density, x is the thickness, ε is the geometrical efficiency and I is the emission probability.

3.2 Scanning equipment

The scanning of a HPGe detector, to create a profile of the deadlayer, is carried out with a scanning station that includes a 30 mm thick and 60 mm high copper collimator with a 1 mm aperture. Herein a 4.29 ± 0.35 MBq ^{241}Am source, made by Eckert & Ziegler Nuclitec, is placed and moved over the detector's endcap while recording counts of one or more gamma peaks. The movement of the collimator is done by a scanner with at least 0.1 mm steps, the scanner is depicted in

Figure 13. After each step a 3 minute measurement is done to acquire a spectrum, in this spectrum the 59 keV line is of particular interest because of its low energy and high emission probability. The results of these measurements create a profile of the detector's deadlayer. Hereafter the scanning is also done for different angles to be sure there are no irregularities. It is also possible to scan the side deadlayer by turning the arm of the scanner 90°. All these measurements are done at the underground laboratory HADES (High Activity Disposal Experimental Site).

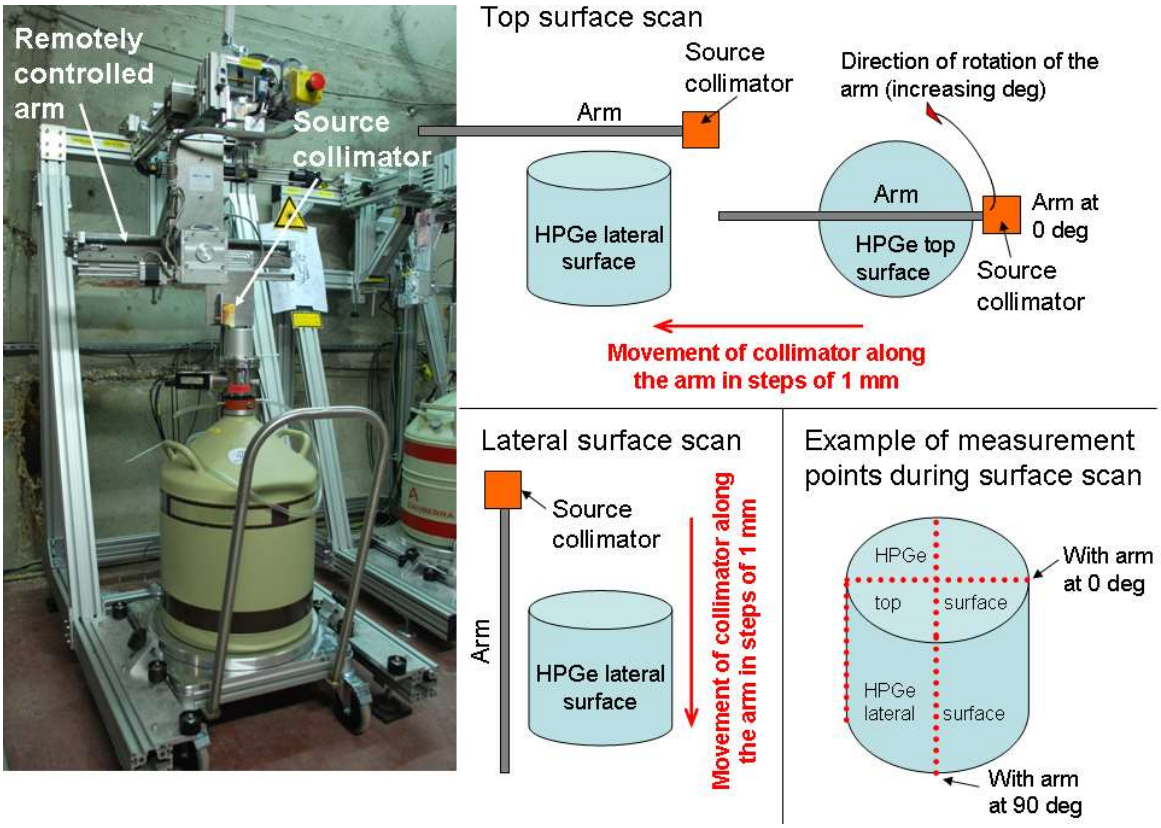

Figure 13: Image of the scanner at HADES together with schematic representation [16, p. 3]

3.2.1 HADES

The scanning of the deadlayers takes place in the underground laboratory HADES (High Activity Disposal Experimental Site). The JRC Geel rents a part of the laboratory where they operate 12 HPGe-detectors and a scanning station. The main reason the scanning station is underground was to be able to scan 35 HPGe detectors that are now used in the GERDA double-beta decay experiment. Since germanium is activated by cosmic rays, the scientists needed to keep the crystals underground as much as possible. Another reason for the scans to take place underground is the use of the 59 keV gamma-ray produced by an ^{241}Am source. If the background was not taken care of the measurement would lose a significant amount of data. Because of the depth the muon flux is reduced by four orders of magnitude and the cosmic ray flux is reduced drastically, this results in a low background.

HADES is located 225 m underground, equivalent to approximately 500 m of water, at the premises of the SCK●CEN and operated by EURIDICE (European Underground Research Infrastructure for DIsposal of nuclear waste in Clay Environment). A schematic drawing of HADES is depicted in Figure 14. To reduce possible microphonic noise the HPGe detectors are placed on separated platforms equipped with vibration dampers.

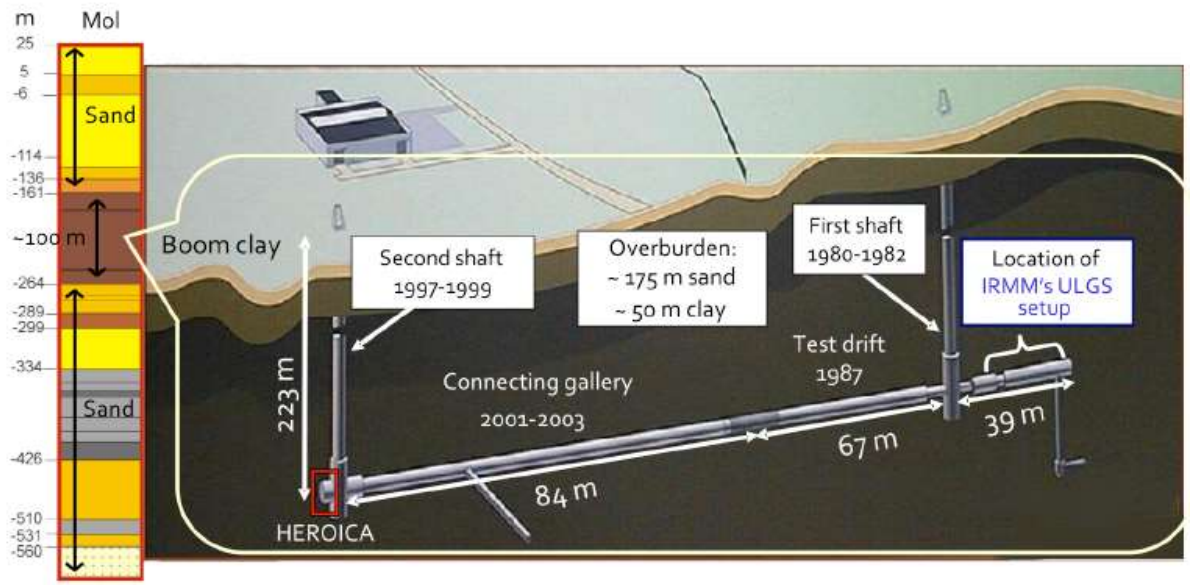

Figure 14: Schematic drawing of the HADES underground labratory, the levels (in m) on the left side are the water equivalent distances [30, p. 3]

Other measures that are taken to decrease the background in radioactivity measurements are the use of an ultra-low-background HPGe detector, a 15-25 cm lead shield of which the inner 2-5 cm is low in ^{210}Pb and finally an inner lining of 1-10 cm of freshly produced electrolytic copper to shield from the radioactivity of the lead. The main sources of background radiation are the following:

- ^{222}Rn concentration and its progenies
- Cosmic ray flux
- Decay of activation products
- Decay of contaminations
- Contamination of sample containers and equipment used for sample preparation

The ^{222}Rn concentration inside the HADES underground laboratory is kept low with a constant ventilation of 10000 m³ air per hour. Because of the ventilation the ^{222}Rn concentration is about the same as for the outside air with a yearly average of 7 Bq/m³ [24]–[30].

3.3 EGSnrc

The models were made with the EGSnrc Monte Carlo code. EGSnrc stands for Electron Gamma Shower National Research Council Canada. This code can model the passage and interactions of electrons and photons with matter. By coding it is possible to create multiple geometries that result in the detector model that is needed. Its original purpose focused on medical physics, but it also can be used for research and development in a wide range of industries and companies that are linked with radiation. The code itself uses C++ geometry libraries to create the needed geometries. As for most Monte Carlo codes a seed must be given to create an array of random numbers. To be sure only the changes in geometry or material are taken into account in this thesis a constant seed is used through all simulations [31].

3.4 Sources

The point sources were produced by PTB (Physikalisch Technische Bundesanstalt, Braunschweig, Germany) and Cerca Framatome LEA (Laboratoire Etalons d'Activité). They are produced by making drop depositions on thin foils and are circular shaped. To position the PTB and LEA sources above the centre of the endcap, custom made PMMA holders are used together with distance rings to get the correct height. On average the diameter of the active area of a source is about 5 mm.

Beside the point sources, a calibration volume source has been used made from a gel placed in a teflon container. The volume source is used to create the energy calibration curves for real environmental samples and contains a mixture of numerous radionuclides to have a wide range of gamma energies. As with the PTB sources, the volume source also has its own custom made PMMA holders and distance rings. The radionuclides in the volume source with their specific activities at the reference date 30/11/2017 are listed in Table 2.

Table 2: Nuclides present in the teflon container with their corresponding specific activities as of 30/11, 2017

Source	Specific Activity (Bq/g)	Uncertainty (Bq/g)
^{241}Am	62.83	0.69
^{133}Ba	22.33	0.27
^{109}Cd	193.42	2.90
^{139}Ce	10.74	0.18
^{57}Co	10.94	0.21
^{60}Co	34.54	0.38
^{51}Cr	264.65	4.50
^{137}Cs	30.84	0.37
^{210}Pb	253.19	3.80
^{241}Am	42.67	0.55
^{133}Ba	50.53	0.76
^{109}Cd	86.5	0.95

3.5 Detectors

In this Master thesis work, five detectors were used: the UHasselt detector from UHasselt, Det28 from the SCK•CEN, and detectors T2, T7 and Ge-6 from the JRC in Geel. Table 3 lists characteristics of the five detectors.

Table 3: Information on all the detectors that were used

	UHasselt detector	**DET28**	**T7**	**T2**	**Ge-6**
Crystal type	Coaxial	Coaxial	Coaxial	Coaxial	coaxial
Manufacturer and model	Oxford, Tennelec/ Nucleus, CPVDS30-20190	Canberra GC4018	Canberra GX6020	Canberra GC2020	Canberra GC8022
Nominal top deadlayer thickness	0.6 mm	0.45 mm	0.3 µm	0.75 mm	1.5 mm
Nominal side deadlayer thickness	0.6 mm	0.45 mm	0.75 mm	1.5 mm	2.0 mm
Crystal to endcap distance (outside)	4 mm	4.5 mm	4 mm	4.25 mm	5.5 mm
Relative efficiency	22.6%	40.4%	62.8%	18.2%	80.5%
FWHM at 1332 keV	1.74 keV	1.78 keV	1.88 keV	1.90 keV	2.15 keV
Crystal height	49.6 mm	61.5 mm	59 mm	31 mm	84 mm
Crystal diameter	51.7 mm	61 mm	71 mm	59 mm	78 mm
Endcap thickness	1.0 mm aluminium	1.5 mm aluminium	1.5 mm aluminium with 0.5 mm carbon epoxy window	0.75 mm aluminium	1.0 mm copper
Endcap diameter	76.2 mm	46.2 mm	89 mm	76.2 mm	95.25 mm
Age at the time of the scanning	21 years	13 years	10 years	No scan was made	No scan was made
Operated by	Hasselt University	SCK•CEN	JRC Geel	JRC Geel	JRC Geel
Other characteristics	Irregular deadlayer	/	Possible yttrium implanted deadlayer	Dented aluminium endcap	/

4 Results and discussion

4.1 Creating models for HPGe detectors

4.1.1 UHasselt detector

The first detector that was modelled was the 21 years old detector of UHasselt. This detector has been kept at room temperature for approximately 70 % of its lifetime. The original deadlayer has a thickness of 0.6 mm as stated by the manufacturer. The endcap is made of aluminium and has a thickness of 1.0 mm. Because it is an old detector and it has been kept at room temperature for more than half its lifetime, the deadlayer should have increased significantly and evenly over the whole detector.

However, the scanning-results showed a different view than anticipated. As can be seen in Figure 15 the deadlayer may have increased over 21 years but certainly not evenly. The scan in Figure 15 was taken at an angle of 60° and the scans at 0° and 120° gave similar results. It is clearly visible that the count-rate pattern shows a "crater" in the middle and a steady downward slope going towards the side. The crater and downward slope indicate an increase in deadlayer thickness, following the logic that a thicker deadlayer results in less active volume and more absorption in the deadlayer, resulting in a lower number of registered counts.

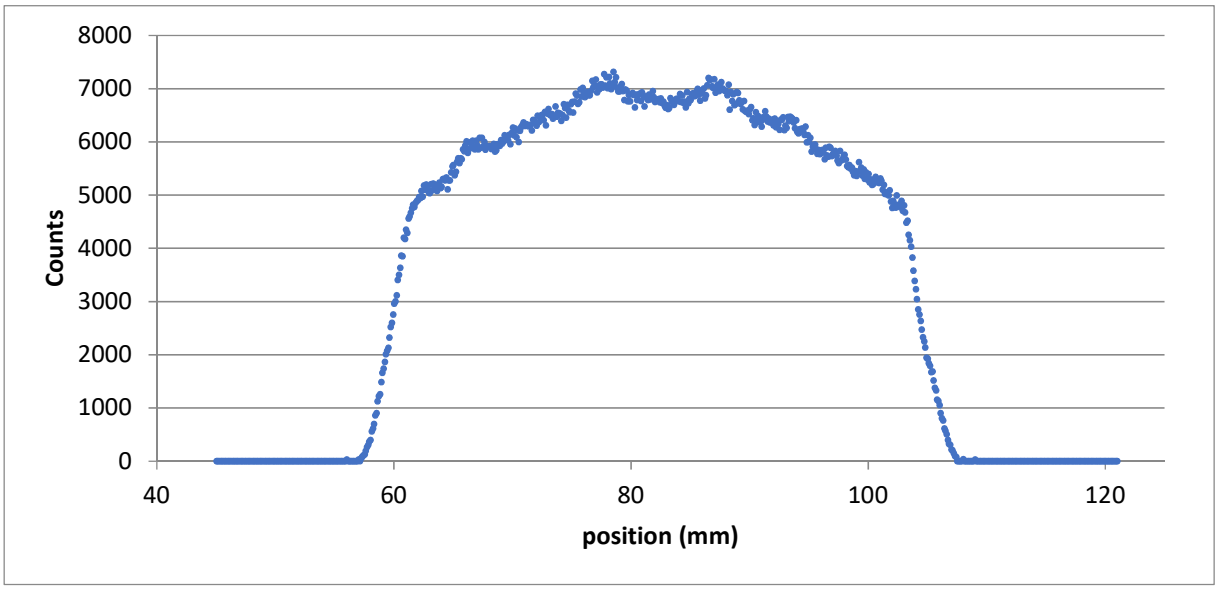

Figure 15: Scan of the detector of UHasselt at an angle of 60°, the scans at 0° and 120° are similar

The origin of the crater in the middle of the scan, shown in Figure 15, could be due to the presence of the bore hole in the germanium crystal. To verify this hypothesis two Monte Carlo models were created. One model had a borehole and the other model did not have a borehole. Figure 16 shows the comparison of both models. The R-squared value of these two curves is equal to 1.000. This gave the confirmation that the existence of the borehole had no significant influence at an energy of 59 keV.

A second reason for the crater could be due to an actual deadlayer that is shaped that way. A possible reason for this particular shape could be that a bias voltage was over the crystal while the crystal itself still was at room temperature. This would increase the diffusion of lithium certainly along the field lines. The borehole also could have an influence on the diffusion process what could give rise to the crater.

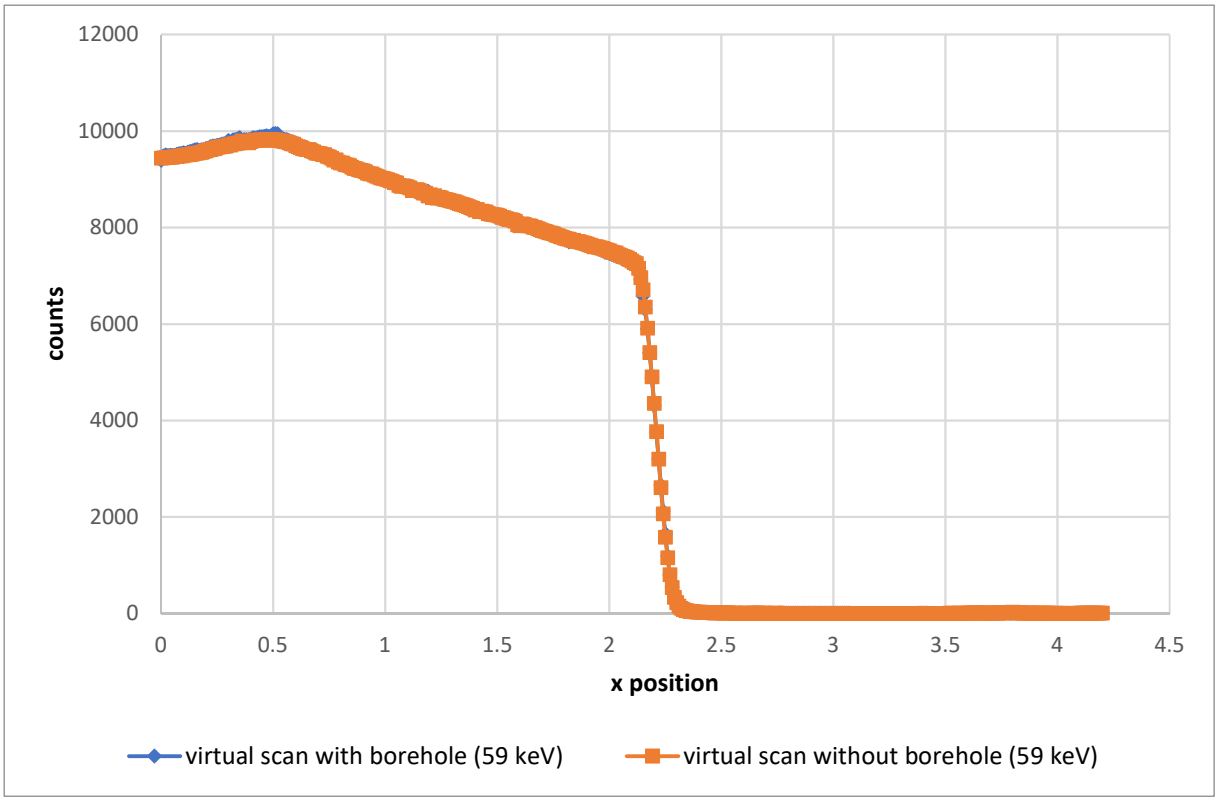

Figure 16: Comparison of a virtual scan with and without borehole to determine the origin of the crater

By contacting the manufacturer info about the bulletization was acquired. However, because of the age of the detector a specific datasheet was not available but an estimated bulletization radius of 3.5 cm was given. To see the impact of this effect, a new model was made without this rounding. The result of the new virtual scan is shown in Figure 17 together with its bulletized form and the real scan. It is visible that there is no significant difference between the two scans. This is in contrast with what is stated in Gasparro et al. [9]. But, the reason why the influence of the bulletization is insignificant here, is the much thicker deadlayer on the side of the crystal. To have a quantifiable result the R-squared of the scan and the model were calculated and also the R-squared of the model and the model with bulletization. This resulted in respectively a R-squared of 0.988 and 1.000.

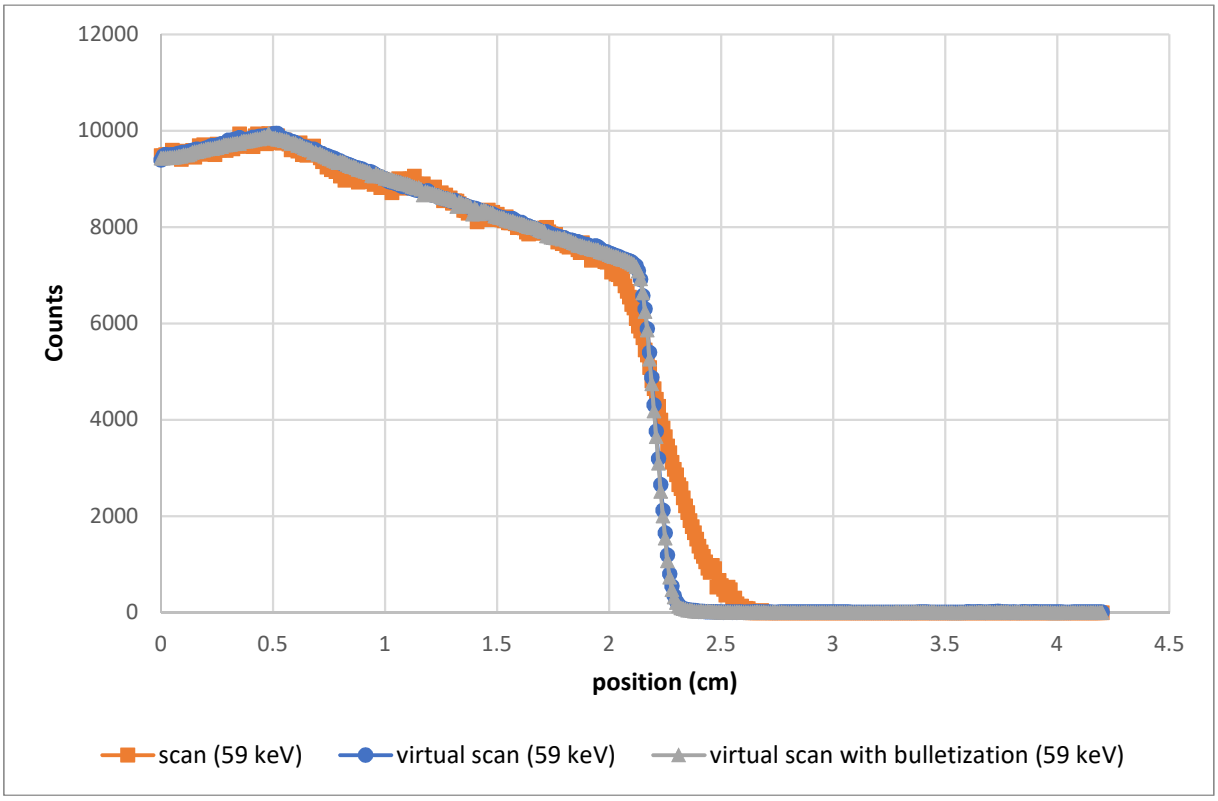

Figure 17: Comparison of the scan made at HADES, the virtual scan without bulletization and the virtual scan with bulletization

To get an idea about the consequences of the irregular deadlayer a second model was made with an evenly distributed deadlayer with thickness equal to the minimum deadlayer of the final model that was made, 0.55 mm. Hereafter, four types of typical samples were simulated: filter, soil, steel and maize. These samples were all cylindrical with t equal to the height of the cylinder. With the acquired results the efficiency of both models was calculated. With both efficiencies the relative difference compared to the final model was calculated and the results are listed in Table 4.

Table 4: Relative difference in efficiency between the model of UHasselt with a flat and an irregular deadlayer for multiple sources

Sample type	**$\Delta\varepsilon$**				
	46.5 keV	**59 keV**	**92.5 keV**	**186 keV**	**662 keV**
Filter (∅ 50 mm, t=2 mm)	73%	43%	20%	8.9%	2.7%
Soil (50 g, ∅ 50 mm, t=40 mm)	67%	40%	19%	8.1%	1.7%
Steel (∅ 50 mm, t=20 mm)	72%	41%	19%	7.7%	1.6%
Maize-powder (50 g, ∅ 50 mm, t=40 mm)	67%	40%	20%	8.0%	1.8%

It is understandable that with higher energies the relative difference becomes less significant, because the deadlayer has less influence with these energies. The results indicate that inhomogeneous deadlayers have a huge impact on the quantification of gamma-rays below 100 keV and are responsible for many discrepancies seen in proficiency tests and probably even in certification of environmental reference materials using intercomparisons.

The final model of the UHasselt detector is schematically given in Figure 18 with all dimensions in mm. The distances of the figure are not to scale to show the overall shape of the deadlayer that otherwise would be too small to see.

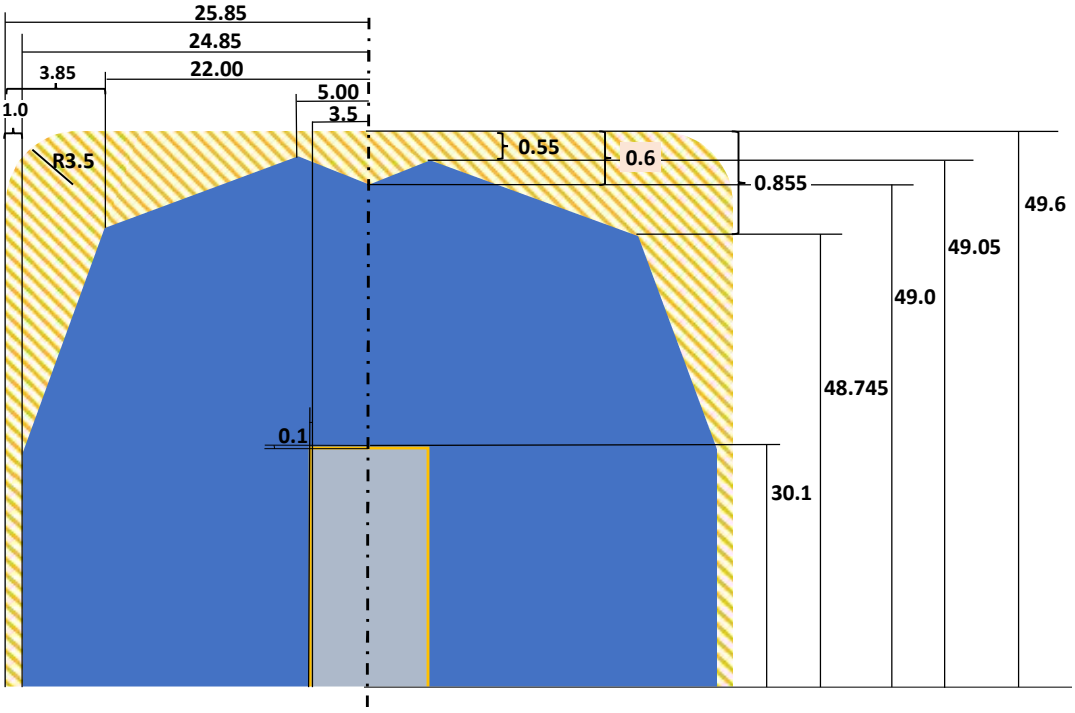

Figure 18: Not to scale model of the detector of UHasselt to show the shape of the deadlayer (mm)

4.1.2 Det28

In collaboration with the SCK•CEN a second detector was scanned and a model was created. The scan is depicted in Figure 19 and is clearly evenly distributed and flat. These conditions make it possible for a first calculation of the deadlayer thickness with the method of Budjas et al. [1] and the method based on the attenuation coefficients. Unfortunately, the first results did not give a conclusive answer as a collimated source was used and a second measurement was not possible due to technical problems with the aluminium endcap of the detector, which necessitated sending it for repair.

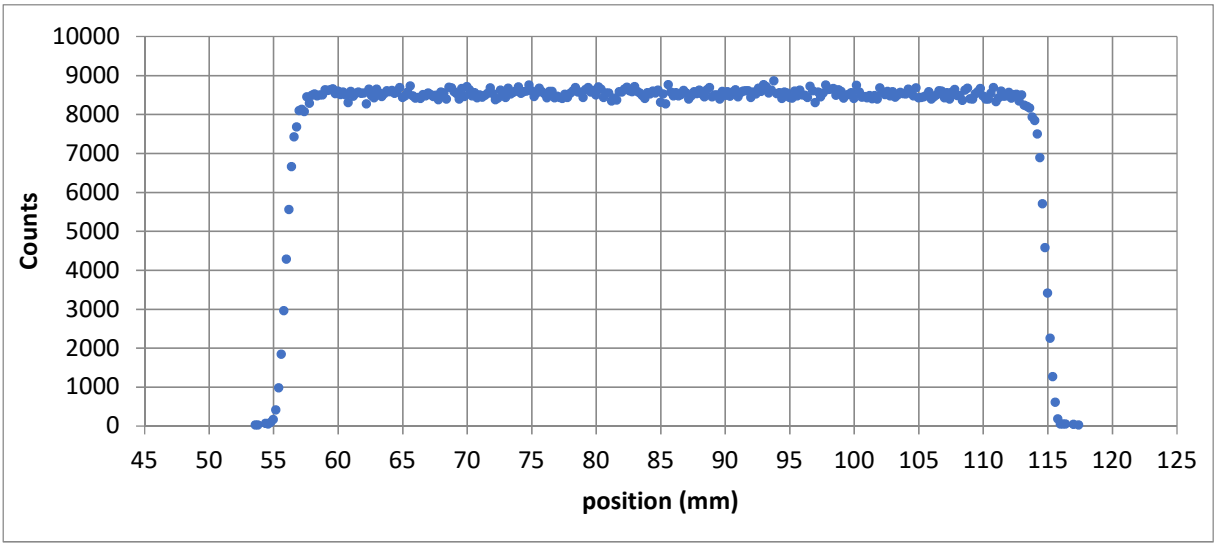

Figure 19: Scan of detector det28 at an angle of 0°, the scans at 60° and 120° are similar

4.1.3 T7

The third detector, detector T7 of the JRC, already had a model but the FEP efficiency of this model had an offset that was considered too large for accurate work. Therefore, a new model was due and a scan was made. T7 is a rather special detector, it has a carbon epoxy entrance window, a deadlayer thickness of 0.3 µm and is bulletized at the bottom of the crystal. In Figure 20 the scan from T7 at an angle of 120° is shown, the scan for 0° and 60° are similar to this one.

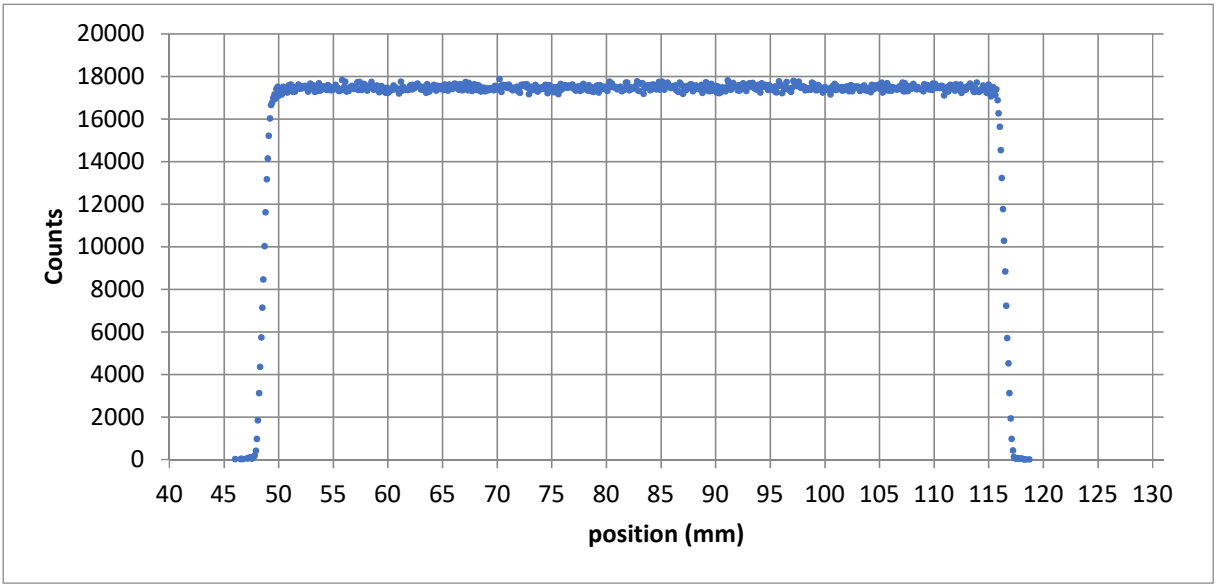

Figure 20: Scan of detector T7 at an angle of 120°, the scans at 0° and 60° are similar

Modelling the carbon epoxy entrance window with a thickness of 0.5 mm was done with the assumption that it was made from a carbon epoxy called polyacrylonitrile or PAN. The problem with this material was that there were no attenuation coefficients available. Therefore, we used the attenuation data obtained with the XCOM-website [32]. For T7, an X-ray was taken and together with the schematics it was confirmed that the crystal had a bulletization at the bottom of the crystal. The origin or reason for the bulletization is unknown.

As mentioned before detector T7 already had a model but the counting efficiency of the simulation with this model had a significant offset compared to the counting efficiency obtained with a reference volume source. Because the counting efficiency calibration will be used for several experiments a new model had to be created. The creation of the new T7 model happened in multiple steps by trial and error. By doing so T7 gave good insight in the influence of the different parameters that were changed. The parameters that were varied are the top deadlayer, the side deadlayer and the endcap to crystal distance. The effects of modifications to the model were investigated by interpretation of the simulation results that are compared with the experimental values. The teflon volume calibration source was kept at a source to endcap distance of 3.50 cm for all measurements. To compare the different modifications to the model the efficiency curve was split into 2 parts, the low region (below 100 keV) and the high energy region (above 100 keV). Splitting the curve in two was needed to better observe the response at high and low energies.

In the charts below the counting efficiency calibration-curves for a volume source are shown for the first and the final (optimised) model. Figure 21 and Figure 22 show respectively the calibration-curve and the relative difference of the first model that corresponds to the geometry as specified by the manufacturer. The relative difference is defined as the experimental efficiency minus the simulated efficiency, divided by the simulated efficiency. The Monte Carlo efficiencies are well below the experimental data obtained with a calibration source. In Figure 23 and Figure 24, respectively the calibration-curve and the relative difference of the final model of T7 are depicted. The calibration data

of the Monte Carlo simulations agree significantly better with the experimental data. The modifications were made to the side deadlayer distance and the endcap to crystal distance. At first the deadlayer thickness was also changed but after numerous attempts it was concluded this could not lead to the correct results while maintaining realistic values. However, the 2734 keV line of ^{88}Y gives a response that does not match with the other energies. After further examination this was due to a lower number of counts what lead to a higher uncertainty.

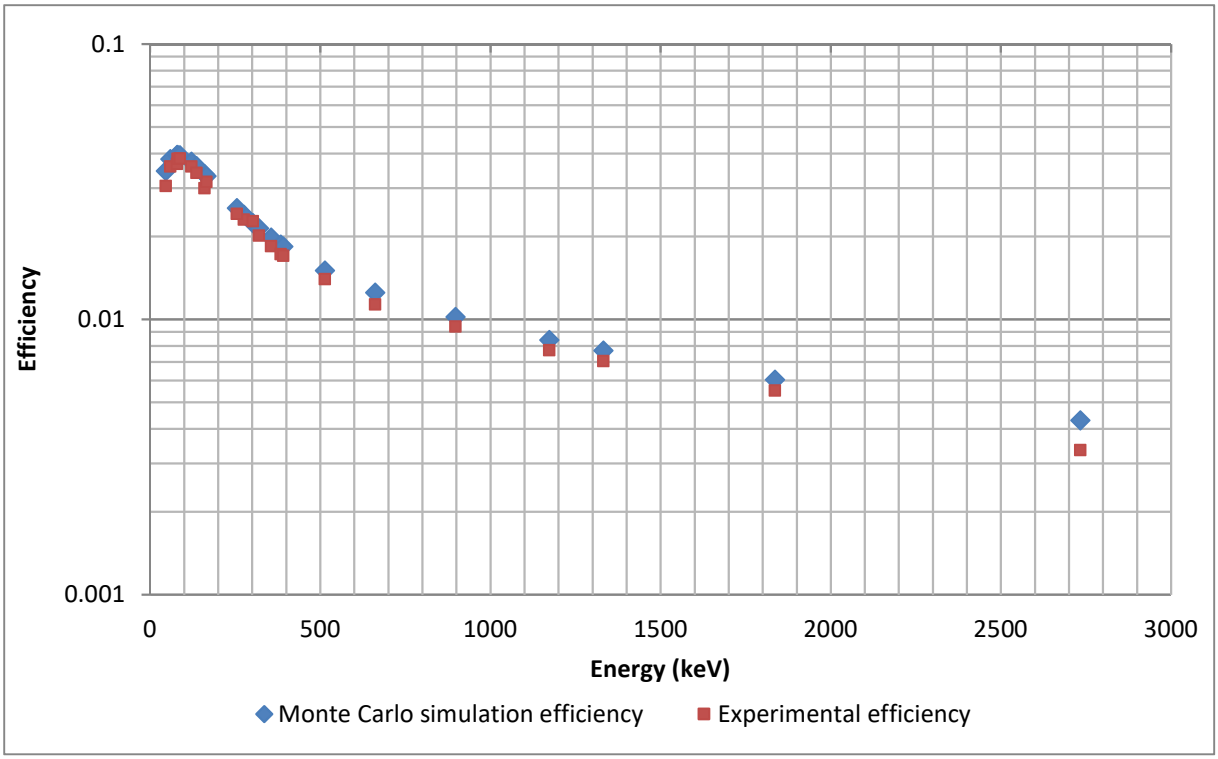

Figure 21: Counting efficiency calibration curve for a volume source with the efficiency in logaritmic scale for model 1 (based on manufacturer data) of detector T7

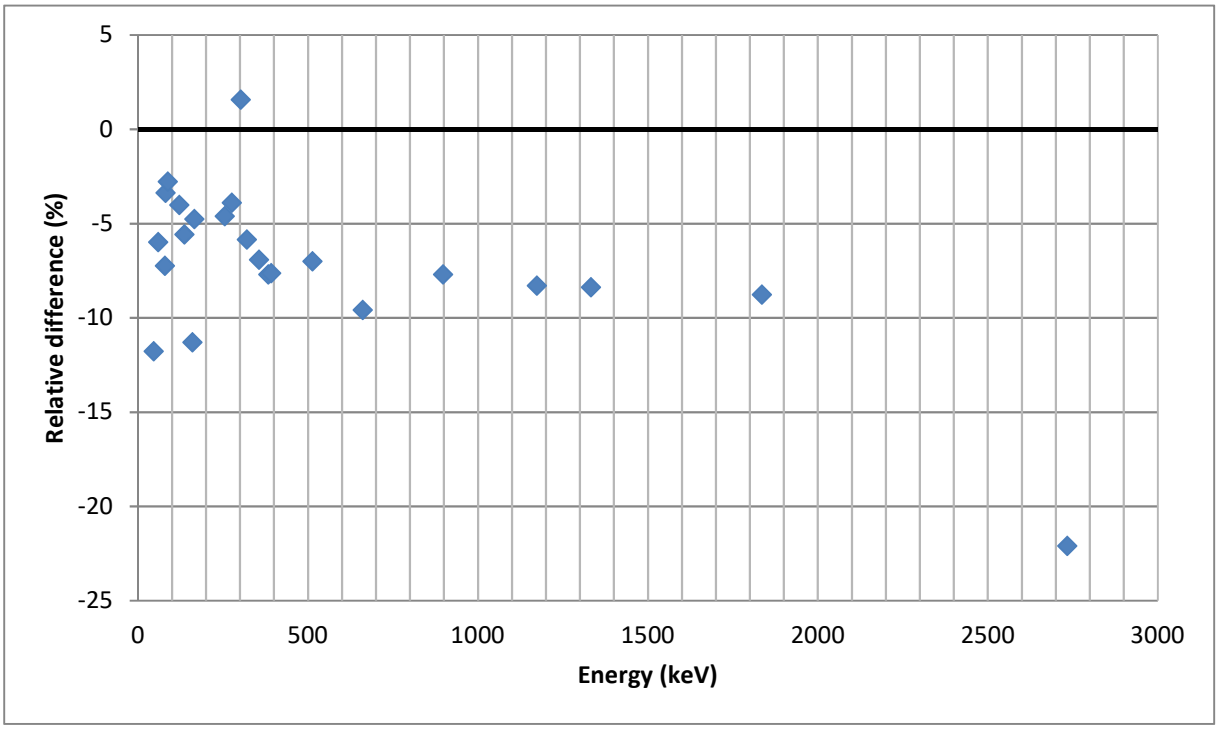

Figure 22: Relative difference ((experimental-simulation)/simulation)(for a volume source) of model 1 (based on manufacturer data) of detector T7

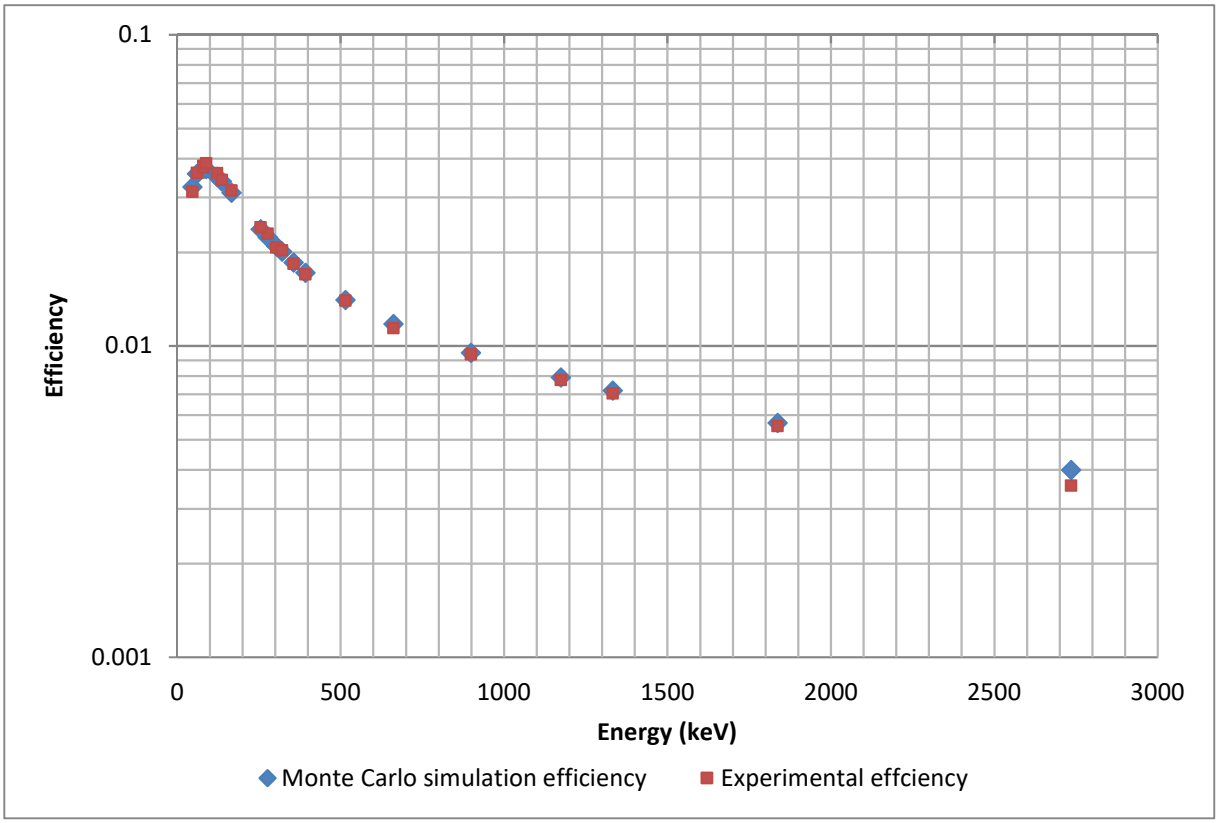

Figure 23: Counting efficiency calibration curve for a volume source with the efficiency in logaritmic scale for model 7 of detector T7

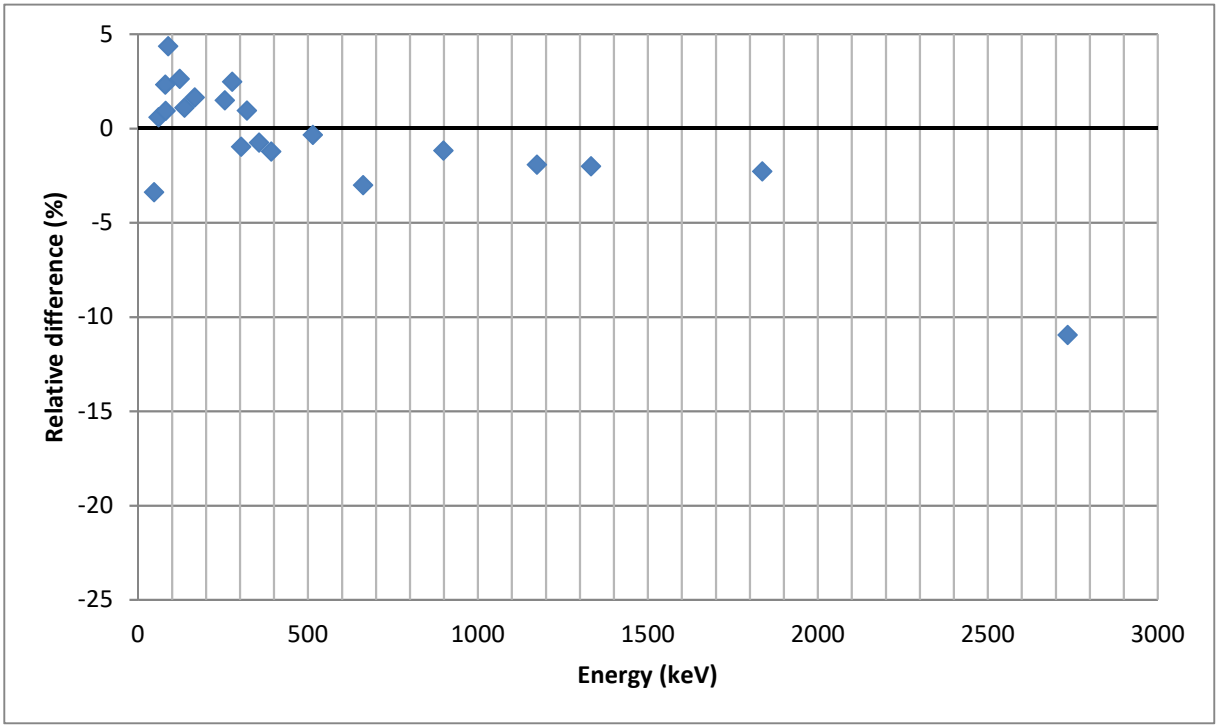

Figure 24: Relative difference ((experimental-simulation)/simulation)(for a volume source) of model 7 (optimised) of detector T7

Table 5 lists the different models that were created with their corresponding modifications and the changes in counting efficiency that these modifications brought forth were split up in a low energy region and a high energy region. As mentioned before, this was to point out that the transformation for both energy regions was not the same. The transformations were always measured with the real measurement as baseline. The first model is the model with the geometry as stated by the manufacturers' datasheet and the last model corresponds to the one that best fits the experimental data. The relative difference between the counting efficiency calibration curves of the simulation and the measurement for the other models are given in ANNEX A.

Table 5: Influence of the change of each parameter on the counting efficiency calibration for detector T7

Model number	Deadlayer thickness (mm)	Endcap to crystal distance (mm)	Side deadlayer thickness (mm)	Mean relative difference for low energy region (%)	Standard deviation on the relative difference for low energies (%)	Mean relative difference for high energy region (%)	Standard deviation on the relative difference for high energies (%)
1	0.0003	4	0.75	-6.22	3.60	-6.49	2.91
2	0.7330	4	0.75	122.72	155.90	-1.21	5.03
3	0.0100	4	0.75	2.59	6.30	-6.43	2.74
4	0.0100	8	0.75	12.50	7.18	2.37	3.14
5	0.0003	7	0.90	1.53	3.86	0.93	2.99
6	0.0003	7	1.00	1.63	4.02	1.46	3.07
7	0.0003	6	1.10	0.96	2.85	-0.23	1.81

The deadlayer thickness of the second model was calculated with the method described by [1] and also with the method based on attenuation. The result of the first method was a deadlayer of 0.733 mm or an increase of almost 2500 times the original deadlayer. The result of the second method was inconclusive. For verification purposes a model with a thick deadlayer was created. It only became clear that the deadlayer still was 0.3 µm thick after numerous attempts.

The deadlayer thickness of 0.3 µm cannot be achieved with lithium diffusion. The manufacturer will not reveal how the thin n+ contact is created. One assumption is that T7 has an yttrium implanted contact that formed the 0.3 µm deadlayer(the assumption is based on finding a patent [33]). Because the yttrium is implanted, the yttrium atoms have replaced the germanium atoms in the crystal lattice (instead of forming interstitials like Li-atoms do) and there is no chance for a significant change in deadlayer thickness over time. Unfortunately, it cannot be confirmed by the manufacturer due to confidentiality. The 0.3 µm deadlayer could also be too thin for the method of Budjas et al. and the method based on attenuation to work, since the counting statistics influenced by the deadlayer are to insignificant.

It is visible in Table 5 that the increase in deadlayer thickness with model 2 had a greater impact on the efficiencies of the lower energies than the higher energies. Model 2 used the deadlayer thickness calculated by the method of Budjas et al. [1], as mentioned earlier this is 0.733 mm.

With the third model the deadlayer thickness was reduced to 0.01 mm. It is clear that compared to the first model the efficiency in the low energy region increased significantly while the change in the high energy region is barely noticeable. Between the third and the fourth model the crystal to endcap distance was increased from 4 mm to 8 mm. The mean relative difference for low and high energies increased approximately an even amount. The fifth and sixth model show the influence of the side deadlayer thickness. With an increase from 0.90 mm to 1.00 mm both the low and high energy region

were affected. However, the influence of this increase was slightly more significant on the high energy compared to the low energy region.

The crystal-to-endcap distance is a geometry parameter while the deadlayer thickness and side deadlayer thickness are linked to material parameters. This causes them to react differently. The crystal-to-endcap distance had an almost even influence on both the energy regions because it was constant for all energies. With the deadlayer thickness and side deadlayer thickness respectively the low energy region and high energy region experienced a larger impact than their counterpart. The main reason behind this effect was the difference in attenuation coefficients and the fact that higher energies will interact more with the side deadlayer because they can penetrate deeper in the crystal.

For the original model following the dimensions of the manufacturer and the final model that corresponds best to the measurement, a counting efficiency for a point source was also compared to a simulation with EGSnrc. Figure 25 and Figure 26 give respectively the calibration-curve and the relative difference of the original model for a point source to endcap distance of 1.3 cm. Figure 27 and Figure 28 give respectively the calibration-curve and relative difference of the final model with that point source to endcap distance. In Table 6 the changes in energy efficiency are shown for both models.

Table 6: Results of the counting efficiency calibration with a point source for detector T7

Model	Mean relative difference for low energy region (%)	Standard deviation on the relative difference for low energies (%)	Mean relative difference for high energy region (%)	Standard deviation on the relative difference for high energies (%)
Original	-3.89	2.37	-8.69	3.30
Final	2.26	2.04	-0.18	1.68

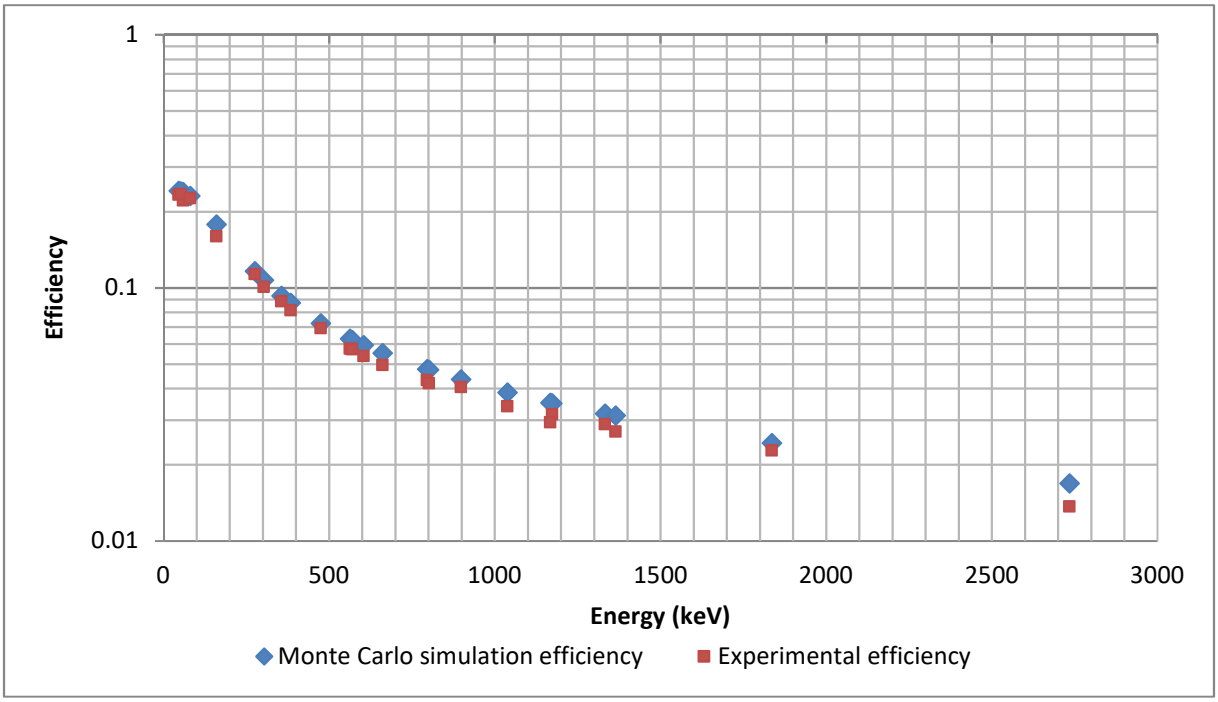

Figure 25: Counting efficiency calibration curve for a point source with the efficiency in logaritmic scale for model 1 of detector T7

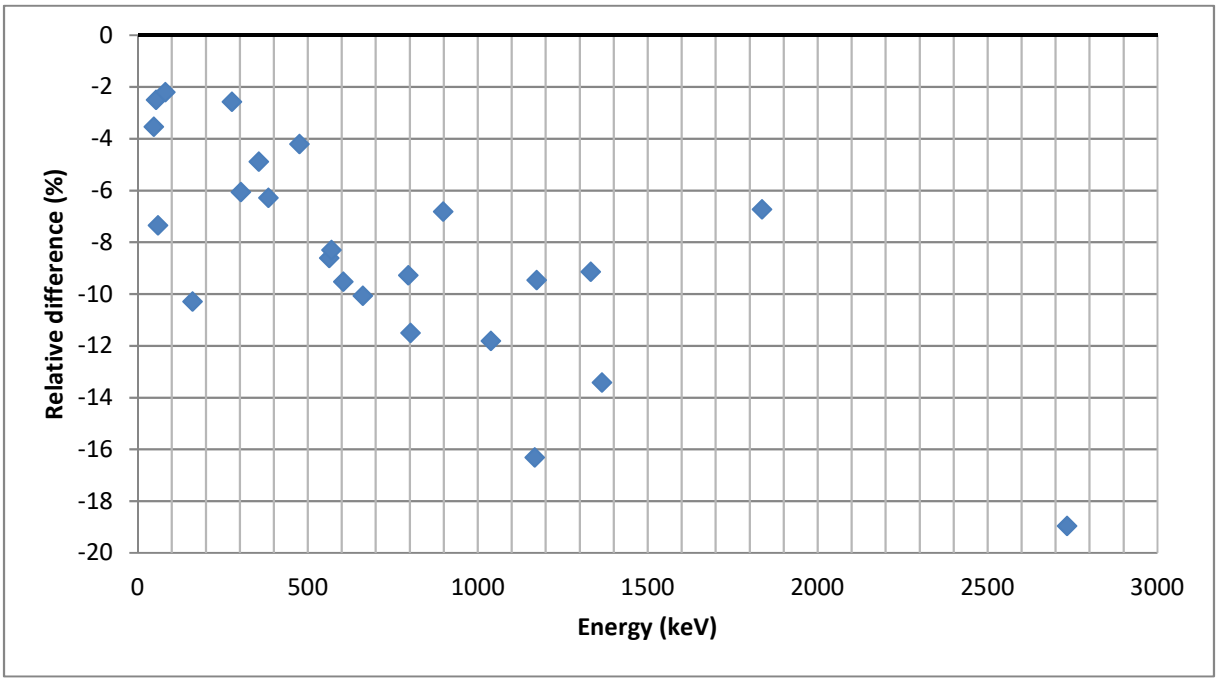

Figure 26: Relative difference ((experimental-simulation)/simulation)(for a point source) of model 1 of detector T7

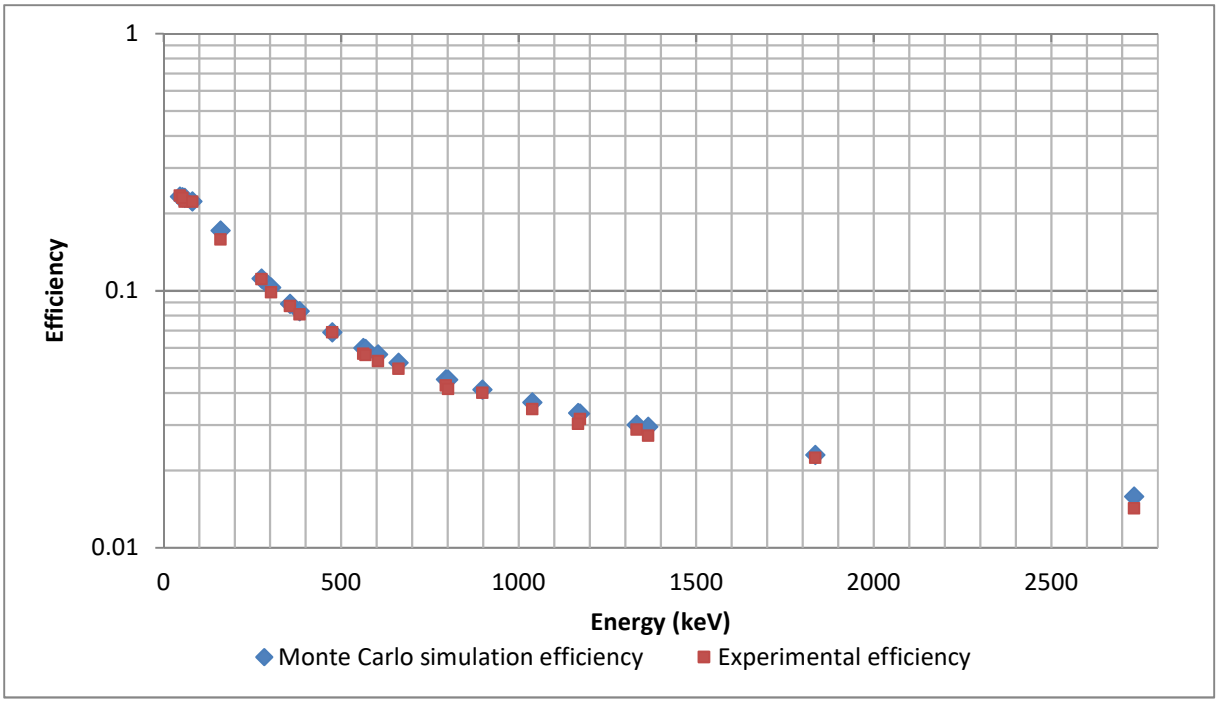

Figure 27: Counting efficiency calibration curve for a point source with the efficiency in logaritmic scale for model 7 of detector T7

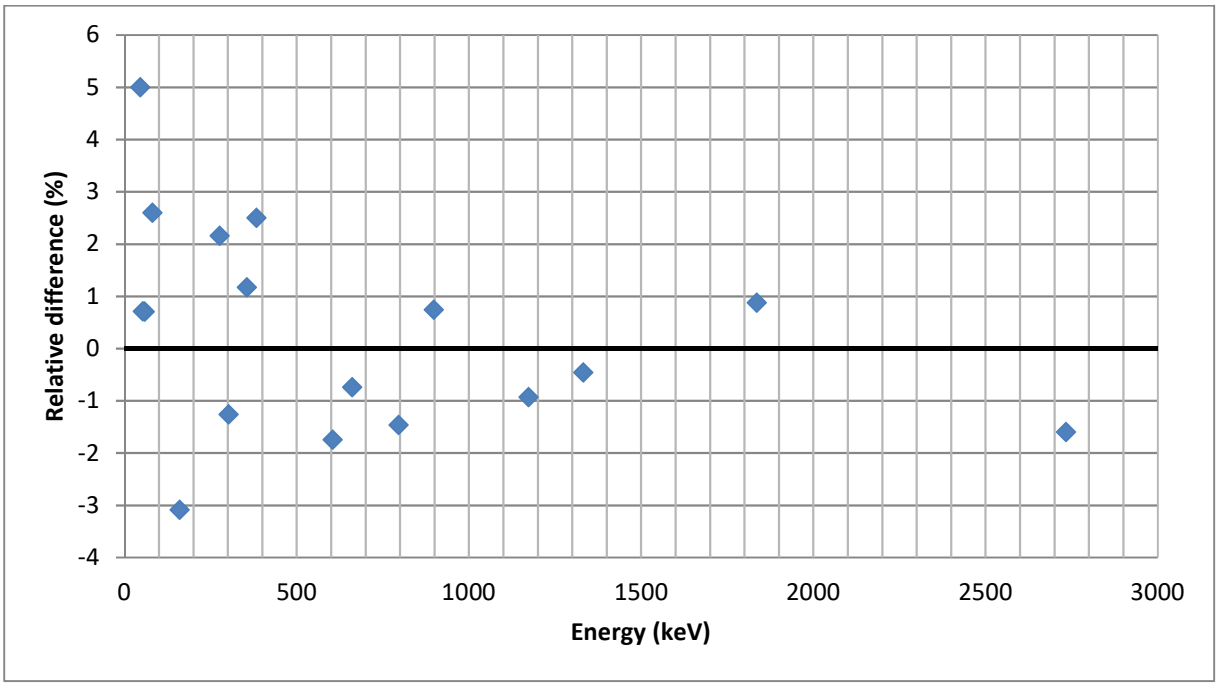

Figure 28: Relative difference ((experimental-simulation)/simulation)(for a point source) of model 7 of detector T7

4.2 Comparison of two deadlayer thickness calculation methods

4.2.1 T2

The fourth detector that was modelled was detector T2. First the method found in Budjas et al. [1] was used with an ^{241}Am point source of 51.6 ± 1.1 kBq and a source to endcap distance of 14.1 cm. A measurement of 66.6 hours was done followed by a gamma analysis with GENIE 2000. The result of this analysis is shown in Table 7. With this data three efficiency ratios were made with the 59 keV peak efficiency as base: One with the sum of the 99 keV and the 103 keV peak; one with only the 99 keV peak and one with only the 103 keV peak. Because T2 has a resolution that can distinguish the 99 keV and the 103 keV peak the summation of these two peaks was not needed but calculations were still done to show how this would affect the final result. The gamma-ray emission probabilities were acquired from the database of DDEP at the website of CEA (Nucleide.org) [34] and are labelled here with an I.

Table 7: Results of the measurement with detector T2 and a 51.6 ± 1.1 kBq ^{241}Am source

	value	uncertainty	relative uncertainty
Counts 59	33652164	5628	0.017
Counts 99	37356	196	0.526
Counts 103	36844	190	0.516
I59	35.92	0.017	(%)
I99	0.0203	0.0004	
I103	0.0195	0.0004	
C59/I59	936864	470	0.001
C99/I99	1840216	37529	0.020
C103/I103	1889436	39966	0.021
R (99+103)/59	3.98	0.06	0.015
R 99/59	1.96	0.04	0.079
R 103/59	2.02	0.04	0.086

Hereafter, five detector models of T2 were made, each with a different top deadlayer thickness. The results of the simulations with those models are shown in Table 8, all the simulations used 50 000 000 events. The results were then used to create three efficiency ratio curves in function of the deadlayer thickness. Figure 29 shows these curves with their trendlines and the functions of these trendlines. The efficiency ratios of the measurements were then entered in the acquired trendline functions that resulted in the deadlayer thicknesses given in Table 9.

Table 8: Results of the simulations with the models of detector T2 with different deadlayer thicknesses

deadlayer thickness (cm)	Counts 59 keV	Counts 99 keV	Counts 103 keV	efficiency 59 keV	efficiency 99 keV	efficiency 103 keV
0.01	321959	338910	337376	0.0064	0.0068	0.0067
0.03	260197	319665	319880	0.0052	0.0064	0.0064
0.05	209494	302026	303403	0.0042	0.0060	0.0061
0.1	122355	260635	264906	0.0024	0.0052	0.0053
0.15	71609	224650	231688	0.0014	0.0045	0.0046

Table 9: Results for the method of Budjas et al. [1] for detector T2

	Efficiency ratio (99+103)/59	Efficiency ratio 99/59	Efficiency ratio 103/59
Deadlayer thickness (mm)	0.898	0.888	0.908
Uncertainty (mm)	0.018	0.025	0.024

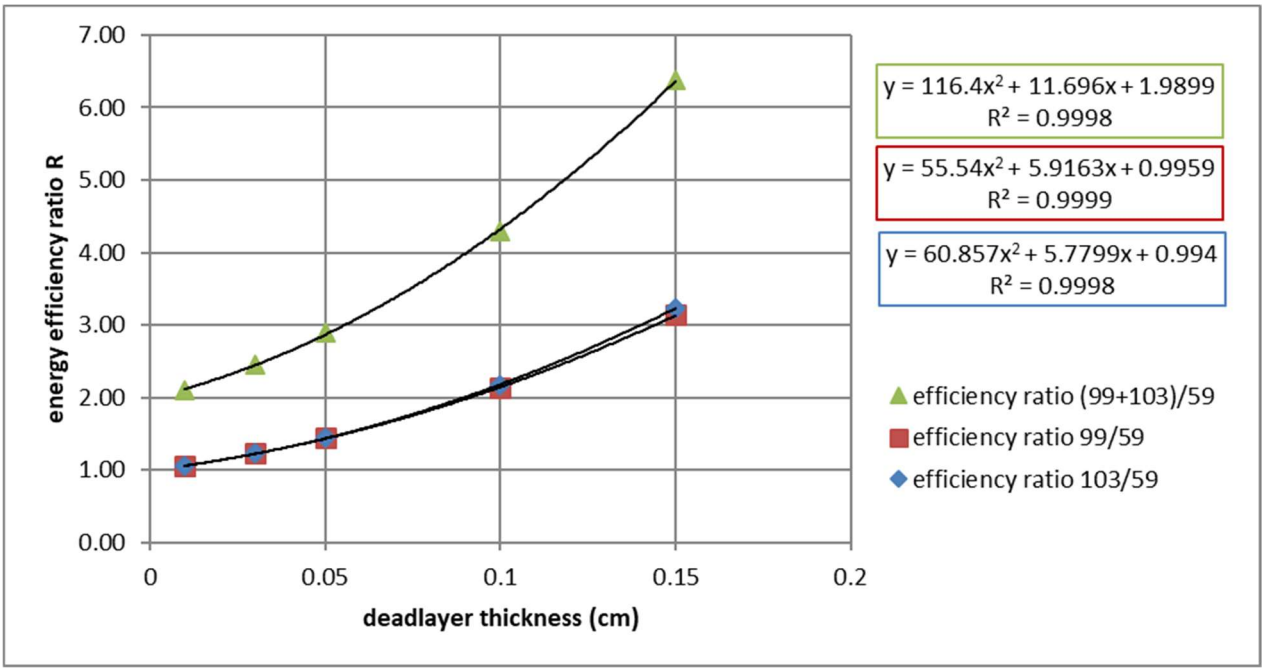

Figure 29: Relative counting efficiency as a function of the deadlayer thickness for detector T2

The second method that was executed is based on the attenuation coefficients. For this method two measurements were done, one with a source to endcap distance of 14.1 cm and one directly on the endcap. The different distances were used to get the influence of the source to endcap distance with this method. Table 10 lists all the values that were needed for the calculation with the source directly on the endcap and for the source at a distance of 14.1 cm. The measurement with the source directly on the endcap took approximately 1 hour with an ^{241}Am point source of 51.6 ± 1.1 kBq and the measurement at a source to endcap distance of 14.1 cm was done with the spectrum of the previous method. The attenuation coefficients were taken from a NIST database [35] and the intensities came from the database of DDEP (Nucleide.org) [34]. The uncertainties of the attenuation coefficients were not given thus a relative uncertainty of 4 % was assumed. The efficiency of the crystal was assumed to be 1 ± 0.01 and the uncertainty on the thickness of the endcap was set to 0.001 cm. The uncertainties of the densities were assumed to be negligible. With equation 10 the deadlayers in Table 11 were calculated together with their uncertainties for the two ratios.

Table 10: Results and values that are needed for the method based on attenuation coefficients for detector T2

	directly on the endcap			at a distance of 14.1 cm		
Energy (keV)	59.54	98.97	102.98	59.54	98.97	102.98
Counts	13548869	19304	20519	33652164	37356	36844
Uncertainty	3745	147	150	5628	196	190
Intensity (%)	35.92	0.0203	0.0195			
μ(Al) (cm²/g)	0.282	0.172	0.168			
μ(DL) (cm²/g)	2.083	0.575	0.537			
ρ(Al) (cm³/g)	2.700	2.700	2.700			
ρ(DL) (cm³/g)	5.323	5.323	5.323			
x(Al) (cm)	0.075	0.075	0.075			
ε	1.00	1.00	1.00			

Table 11: Results for the method based on attenuation coefficients for detector T2

	59/99		59/103	
	on endcap	**at 14.1 cm**	**on endcap**	**at 14.1 cm**
Deadlayer thickness (mm)	1.124	0.813	1.218	0.824
Uncertainty (mm)	0.072	0.056	0.075	0.055
Mean (mm)	0.969		1.021	
Uncertainty mean (mm)	0.046		0.047	

The difference between the two measurements for each ratio is due to the difference in the angle of the gamma-rays. The method based on attenuation takes an average deadlayer thickness and with a measurement close to the detector the average angle of the incident gamma-rays is larger than with a measurement at a larger distance. This gives a thicker deadlayer because the gamma-rays going to the edge of the detector will cross the deadlayer diagonal. This phenomenon is also shown in Figure 9.

The values of Table 9 and Table 11 were used for a counting efficiency calibration. This calibration agreed best with the measurement with a deadlayer thickness equal to the mean of the method of Budjas et al. [1], namely 0.90 mm. The relative difference between the energy calibration curve of the simulation and the measurement of T2 can be found in ANNEX B and was done for simulations with the original deadlayer thickness from the manufacturers datasheet, the two calculated deadlayer thicknesses and the mean of these calculated deadlayer thicknesses.

4.2.2 Ge-6

The measurements and calculations that were done with detector T2 were also done with detector Ge-6. The main difference between the two detectors is the material of the endcap. T2 has an aluminium endcap, while Ge-6 has a copper endcap. This was certainly important with the method based on attenuation coefficients because they had to be adjusted. For the method in Budjas et al. [1] no changes were needed and the same measurements as with T2 were done.

The method of Budjas et al. was executed first. Analogue to T2 five models were made with each a different deadlayer thickness and a measurement with an ^{241}Am source of 51.6 ± 1.1 kBq at a source to endcap distance of 14.6 cm was done. The simulations all used again 50 000 000 events. With the acquired data, listed in Table 12 and Table 13 the three energy efficiency ratios were calculated and the according trendlines for each ratio were created out of the simulation data. These trendlines are shown in Figure 30 together with their functions.

Table 12: Results of the simulations with the models of detector Ge-6 with different deadlayer thicknesses

deadlayer thickness (cm)	Counts 59 keV	Counts 99 keV	Counts 103 keV	efficiency 59 keV	efficiency 99 keV	efficiency 103 keV
0.05	96035	364051	377280	0.0019	0.0073	0.0075
0.1	55453	313398	329310	0.0011	0.0063	0.0066
0.15	32395	270190	287586	0.0006	0.0054	0.0058
0.2	18535	232527	250956	0.0004	0.0047	0.0050
0.25	10971	201024	218761	0.0002	0.0040	0.0044

Table 13: Results of the measurement with detector Ge-6 and a 51.6 ± 1.1 kBq ^{241}Am source

	value	uncertainty	Relative uncertainty
Counts 59	11835845	3518	0.030
Counts 99	47609	270	0.567
Counts 103	54143	256	0.472
I59	35.92	0.017	(%)
I99	0.0203	0.0004	
I103	0.0195	0.0004	
C59/I59	329506	184	0.0006
C99/I99	2345267	48089	0.0205
C103/I103	2776559	58443	0.0210
R (99+103)/59	15.54	0.23	0.0148
R 99/59	7.12	0.15	0.0205
R 103/59	8.43	0.18	0.0211

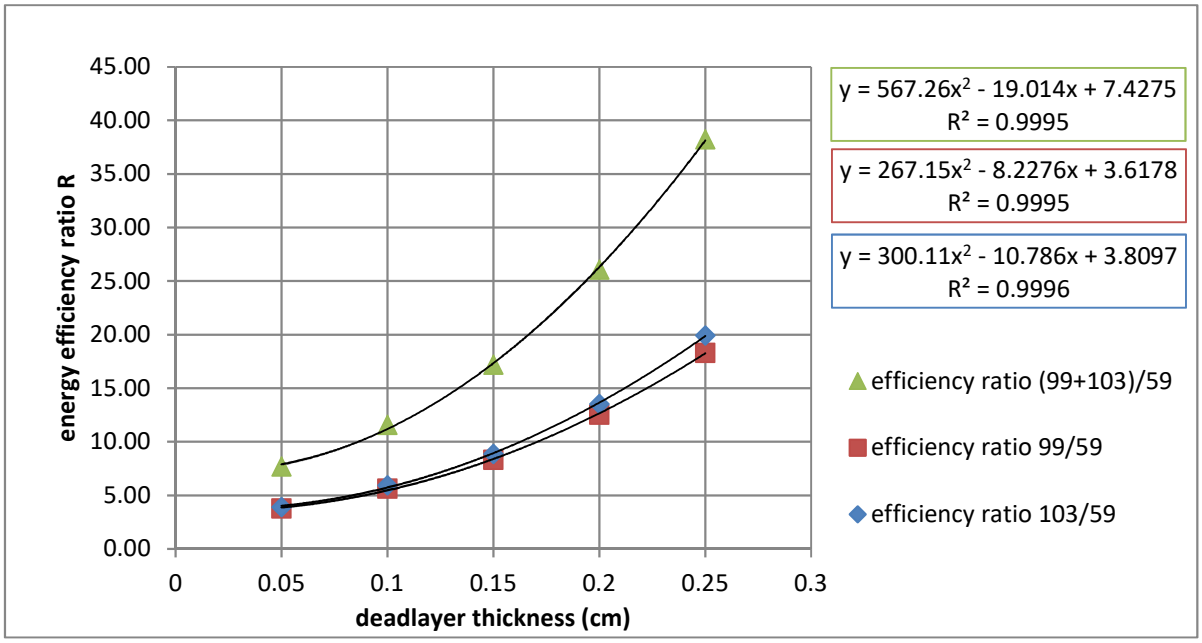

Figure 30: Relative counting efficiency as a function of the deadlayer thickness for detector Ge-6

The efficiency ratios obtained were inserted in these functions and resulted in the values tabulated in Table 14.

Table 14: Results for the method of Budjas et al. [1] for detector Ge-6

	Efficiency ratio (99+103)/59	Efficiency ratio 99/59	Efficiency ratio 103/59
Deadlayer thickness (mm)	1.375	1.309	1.433
Uncertainty (mm)	0.017	0.024	0.024

The method based on attenuation coefficients was also used with this detector. Two measurements were done, one at a source to endcap distance of 14.5 cm and a ^{241}Am source of 53.1 ± 1.1 kBq. And a second one with a source to endcap distance of 1.3 cm and a 241Am source of 11,71 ± 0.12 kBq. With the second measurement a different, less active source was needed because of the deadtime. The results of these measurements together with other values that are needed for equation 10 are tabulated in Table 15.

Table 15: Results and values that are needed for the method based on attenuation coefficients for detector Ge-6

	at a distance of 1.3 cm			at a distance of 14.5 cm		
Energy (keV)	59.54	98.97	102.98	59.54	98.97	102.98
Counts	8304695	55124	61194	11835845	47609	54143
Uncertainty	2927	284	275	3518	270	256
Intensity (%)	35.920	0.0203	0.0195			
μ(Cu) (cm²/g)	1.640	0.474	0.444			
μ(DL) (cm²/g)	2.083	0.575	0.537			
ρ(Cu) (cm³/g)	8.960	8.960	8.960			
ρ(DL) (cm³/g)	5.323	5.323	5.323			
x(Cu) (cm)	0.1	0.1	0.1			
ε	1.00	1.00	1.00			

With the aid of equation 10 the deadlayers listed in Table 16 were calculated and the same assumptions as with detector T2 were taken.

Table 16: Results for the method based on attenuation coefficients for detector Ge-6

	59/99		59/103	
	at 1.3 cm	**at 14.5 cm**	**at 1.3 cm**	**at 14.5 cm**
Deadlayer thickness (mm)	1.768	1.144	1.867	1.288
Uncertainty (mm)	0.131	0.087	0.132	0.085
Mean (mm)	1.456		1.578	
Uncertainty mean (mm)	0.079		0.079	

The values of Table 14 and Table 16 were again compared to the deadlayer value that gave the best counting efficiency calibration, namely 1.5 mm. This deadlayer thickness agreed best to the mean obtained via the method based on attenuation, namely 1.456 mm and 1.578 mm. The relative difference between the energy calibration curve of the simulation and the measurement of Ge-6 can be found in. Because the counting efficiency calibration with this deadlayer resulted in small relative differences, under 5%, the other deadlayer thicknesses were not tested.

5 Conclusion

The shape of the count-rate scan of the detector of UHasselt had an irregular symmetrical deadlayer with a "crater" in the middle of the crystal and a steady downward slope going to the edge. This “crater” means that a thicker deadlayer is present in the middle. The origin of this shape is most likely due to Li-diffusion in preferential directions creating an inhomogeneous deadlayer thickness. However, the reduced active volume because of the borehole is excluded as possible cause of the crater. The low energy gamma-rays used in the scan cannot penetrate deep enough for this to have an effect. This detector should not be used for high accuracy measurements because of its complex deadlayer.

The process of creating a new improved model of detector T7 gave insight in the influence of the different parameters that can be adapted. The iterative optimisation process (shown in Figure 10) that was used proved to be successful and by splitting the efficiency calibration curve in two regions, a low and high region, the separate response of these two regions was measured. The low and high region were both influenced a similar amount by changing the endcap to crystal distance. For the deadlayer thickness this was not the case. Here the low energy region experienced a larger change than the high energy region. For the side deadlayer thickness the opposite was true and the high energy region experienced a larger change. This is due to the fact that the higher energies can penetrate deep enough to be affected by the side deadlayer while this is not the case for the lower energies.

Using detector T2 and Ge-6 two types of deadlayer thickness calculations methods were compared. The first method that is described in Budjas et al. [1] is based on the difference in efficiency between two or more energies of the same radionuclide. The second method is based on the difference in attenuation coefficients between two or more energies. The deadlayer thicknesses that were found were approximately the same if their error was taken into account. In any case, a counting efficiency calibration should still be executed to determine which modelled deadlayer gives the best agreement when compared to a measurement of a reference source. However, it is important to notice that these values do not represent a physical deadlayer thickness but rather generate a deadlayer thickness that agrees best to the response of the detector. The results of these two detectors invoke the need for a more thorough study of both methods to increase their accuracy.

References

[1] D. Budjáš, M. Heisel, W. Maneschg, and H. Simgen, “Optimisation of the MC-model of a p-type Ge-spectrometer for the purpose of efficiency determination,” *Appl. Radiat. Isot.*, vol. 67, no. 5, pp. 706–710, 2009.

[2] Pixeo and SCK-CEN, “SCK•CEN,” *2017*, 2017. [Online]. Available: http://sck.cen.be/. [Accessed: 16-Oct-2017].

[3] SCK•CEN, “SCK•CEN Belgian Nuclear Research Centre,” 2012.

[4] G. R. Gilmore, *Practical Gamma-ray Spectrometry*, Second. John Wiley & Sons, 1996.

[5] H. Spieler, *Semiconductor Detector Systems*. Oxford: Oxford university press, 2005.

[6] G. E. Knoll and J. Wiley, *Radiation Detection and Measurement Third Edition*, Third. Michigan: John Wiley & Sons, 2000.

[7] E. Aguayo *et al.*, “Characteristics of signals originating near the lithium-diffused N+ contact of high purity germanium p-type point contact detectors,” *Nucl. Instruments Methods Phys. Res. Sect. A Accel. Spectrometers, Detect. Assoc. Equip.*, vol. 701, pp. 176–185, 2013.

[8] G. Lutter *et al.*, “Measurement of anthropogenic radionuclides in post-Fukushima Pacific seawater samples,” *Nukleonika*, vol. 60, no. 3, pp. 545–550, 2015.

[9] J. Gasparro, M. Hult, P. N. Johnston, and H. Tagziria, “Monte Carlo modelling of germanium crystals that are tilted and have rounded front edges,” *Nucl. Instruments Methods Phys. Res. Sect. A Accel. Spectrometers, Detect. Assoc. Equip.*, vol. 594, no. 2, pp. 196–201, 2008.

[10] M. B. Challan, “Gamma-ray efficiency of a HPGe detector as a function of energy and geometry,” *Appl. Radiat. Isot.*, vol. 82, pp. 166–169, 2013.

[11] P. Tayyebi, F. Abbasi Davani, M. Tabasi, and H. Afarideh, “A novel technique for detection efficiency determination of HPGe,” *Radiat. Phys. Chem.*, vol. 133, no. August 2016, pp. 86–90, 2017.

[12] Q. Looker, M. Amman, and K. Vetter, “Leakage current in high-purity germanium detectors with amorphous semiconductor contacts,” *Nucl. Instruments Methods Phys. Res. Sect. A Accel. Spectrometers, Detect. Assoc. Equip.*, vol. 781, pp. 20–25, 2015.

[13] CANBERRA, “Germanium Detectors Manual,” 2003.

[14] Ortec, “The Best Choice of High Purity Germanium (HPGe) Detector,” South Illinois.

[15] P. Dryak, P. Kovar, and A. Gudelis, “Total efficiency of GE detectors-dead layer signal effect,” *Appl. Radiat. Isot.*, vol. 68, no. 7–8, pp. 1451–1453, 2010.

[16] E. Andreotti *et al.*, “Determination of dead-layer variation in HPGe detectors,” *Appl. Radiat. Isot.*, vol. 87, pp. 331–335, 2014.

[17] P. N. Johnston, M. Hult, and J. Gasparro, “Cascade summing effects in close geometry gamma-ray spectrometry,” *Appl. Radiat. Isot.*, vol. 64, no. 10–11, pp. 1323–1328, 2006.

[18] M. Hult, “Low-level gamma-ray spectrometry using Ge-detectors,” vol. 87, 2007.

[19] A. N. Berlizov and V. V. Tryshyn, “A Monte Carlo approach to true-coincidence summing correction factor calculation for gamma-ray spectrometry applications,” *J. Radioanal. Nucl. Chem.*, vol. 264, no. 1, pp. 169–174, 2005.

[20] R. Shweikani, M. Hasan, and M. Takeyeddin, “A simplified technique to determine random coincidence summing of gamma rays and dead time count loss corrections,” *Appl. Radiat. Isot.*, vol. 82, pp. 72–74, 2013.

[21] R. Lindstrom and R. Fleming, “Dead time, pileup, and accurate gamma-ray spectrometry,” *Radioact. Radiochem.*, vol. 6, no. 2, pp. 20–27, 1995.

[22] P. C. Ortiz-Ramirez, “Development of an absolute method for efficiency calibration of a coaxial HPGe detector for large volume sources,” *Nucl. Instruments Methods Phys. Res. Sect. A Accel. Spectrometers, Detect. Assoc. Equip.*, vol. 793, pp. 49–56, 2015.

[23] M. Y. Kang, G. M. Sun, J. Kim, and H. D. Choi, “Determination of HPGe peak efficiency for voluminous gamma-ray sources by using an effective solid angle method,” *Appl. Radiat. Isot.*, vol. 116, pp. 69–76, 2016.

[24] G. Lutter *et al.*, “A new versatile underground gamma-ray spectrometry system,” *Appl. Radiat. Isot.*, vol. 81, pp. 81–86, 2013.

[25] M. Hult *et al.*, “Underground search for the decay of Ta180m,” *Phys. Rev. C - Nucl. Phys.*, vol. 74, no. 5, pp. 1–5, 2006.

[26] M. Hult, J. Gasparro, P. N. Johnston, and M. Köhler, “Underground Measurements of Environmental Radioactivity: European Examples,” vol. 1, pp. 18–23, 2003.

[27] M. Hult, G. Lutter, A. Yüksel, G. Marissens, M. Misiaszek, and U. Rosengård, “Comparison of background in underground HPGe-detectors in different lead shield configurations,” *Appl. Radiat. Isot.*, vol. 81, pp. 103–108, 2013.

[28] “Het ondergrondse laboratorium HADES | Euridice.” [Online]. Available: http://www.euridice.be/nl/content/het-ondergrondse-laboratorium-hades. [Accessed: 27-Feb-2018].

[29] M. Hult, M. J. Martínez Canet, M. Köhler, J. Das Neves, and P. N. Johnston, “Recent developments in ultra low-level γ-ray spectrometry at IRMM,” *Appl. Radiat. Isot.*, vol. 53, no. 1–2, pp. 225–229, 2000.

[30] E. Andreotti *et al.*, “HEROICA: An underground facility for the fast screening of germanium detectors,” *J. Instrum.*, vol. 8, no. 6, 2013.

[31] C. National Research Council, “EGSnrc,” 2015. [Online]. Available: https://www.nrc-cnrc.gc.ca/eng/solutions/advisory/egsnrc_index.html. [Accessed: 05-May-2018].

[32] “NIST XCOM: Element/Compound/Mixture.” [Online]. Available: https://physics.nist.gov/PhysRefData/Xcom/html/xcom1.html. [Accessed: 21-May-2018].

[33] E. Hull, R. Pehl, B. Suttle, and J. Lathrop, “Patent Yttrium deadlayer,” 2014.

[34] Laboratoire National Henri Becquerel, “LaraOnTheWeb,” 2017. [Online]. Available: http://www.nucleide.org/Laraweb/index.php. [Accessed: 20-Jan-2018].

[35] NIST, “Attenuation data NIST,” 2017. [Online]. Available: https://www.nist.gov/pml/x-ray-mass-attenuation-coefficients. [Accessed: 08-Apr-2018].

ANNEX

ANNEX A: counting efficiency calibration-curves for the computer models of detector T7

Model 2

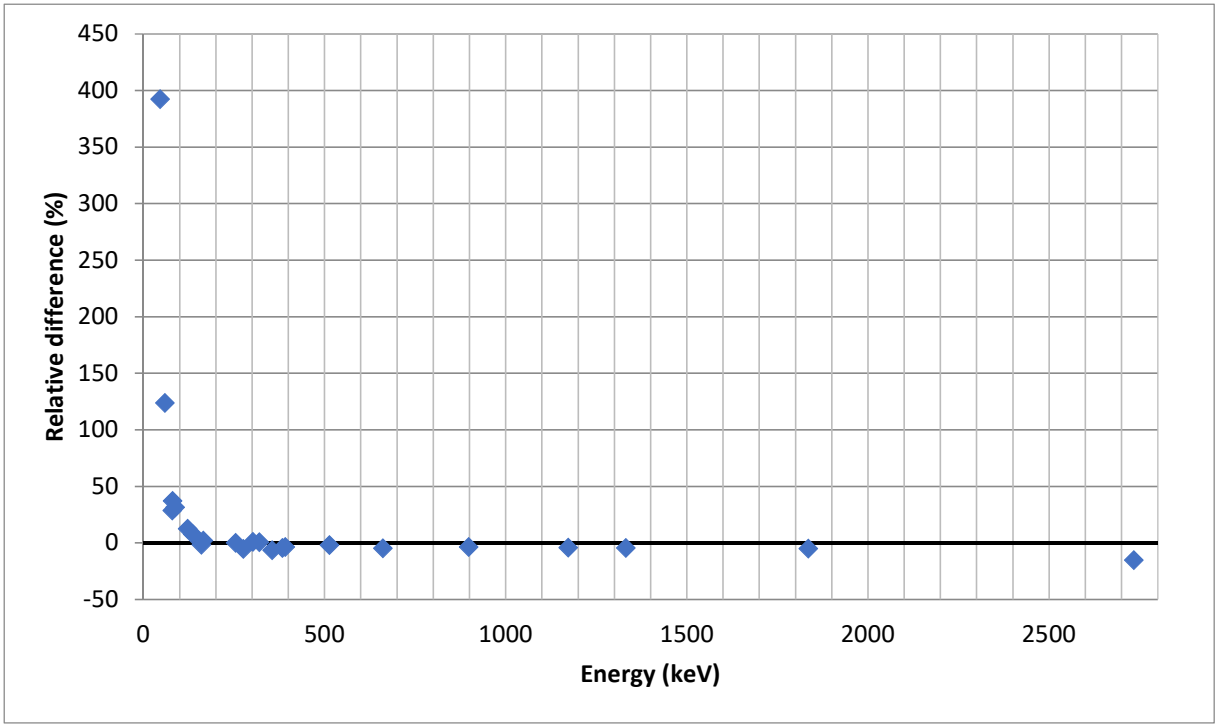

Figure 31: Relative difference ((experimental-simulation)/simulation)(for a volume source) of model 2 of detector T7

Model 3

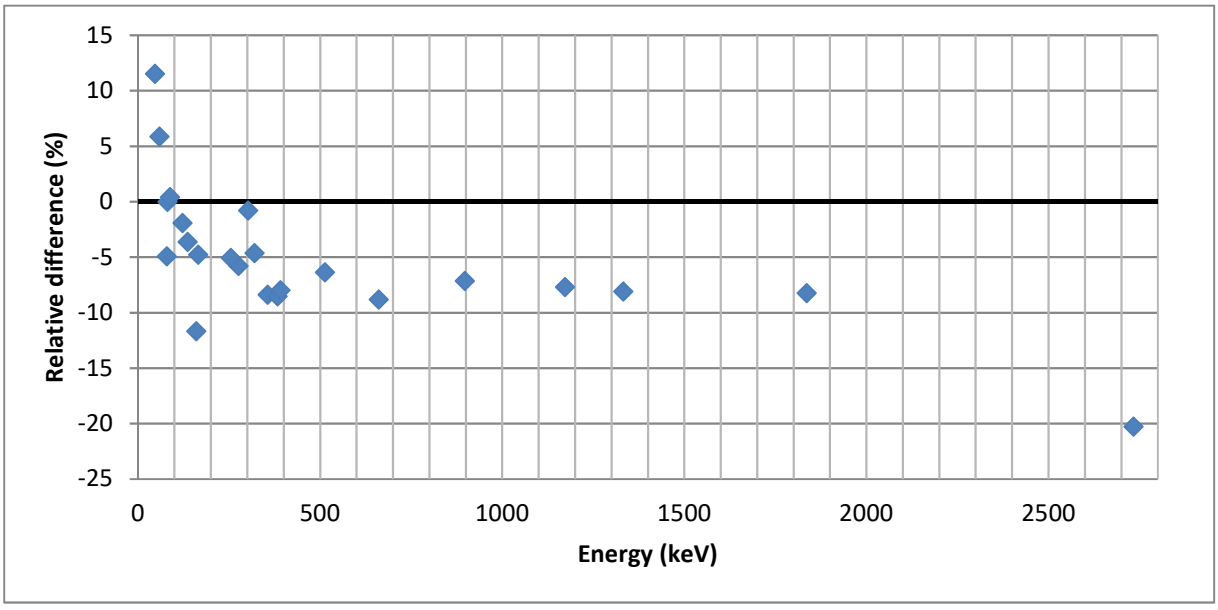

Figure 32: Relative difference ((experimental-simulation)/simulation)(for a volume source) of model 3 of detector T7

Model 4

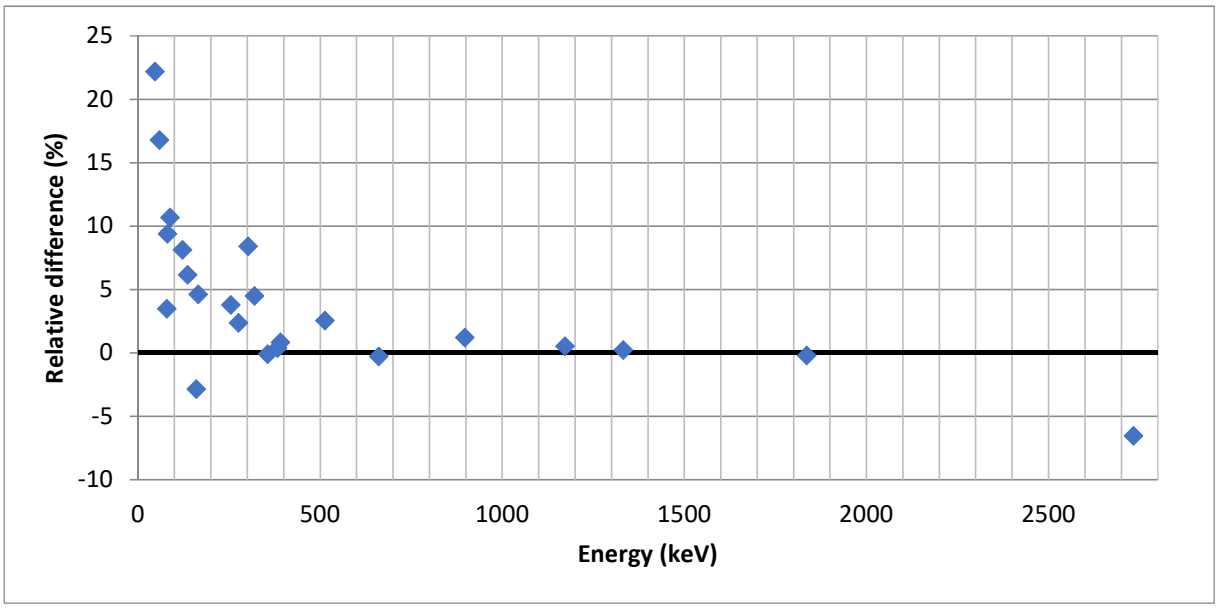

Figure 33: Relative difference ((experimental-simulation)/simulation)(for a volume source) of model 4 of detector T7

Model 5

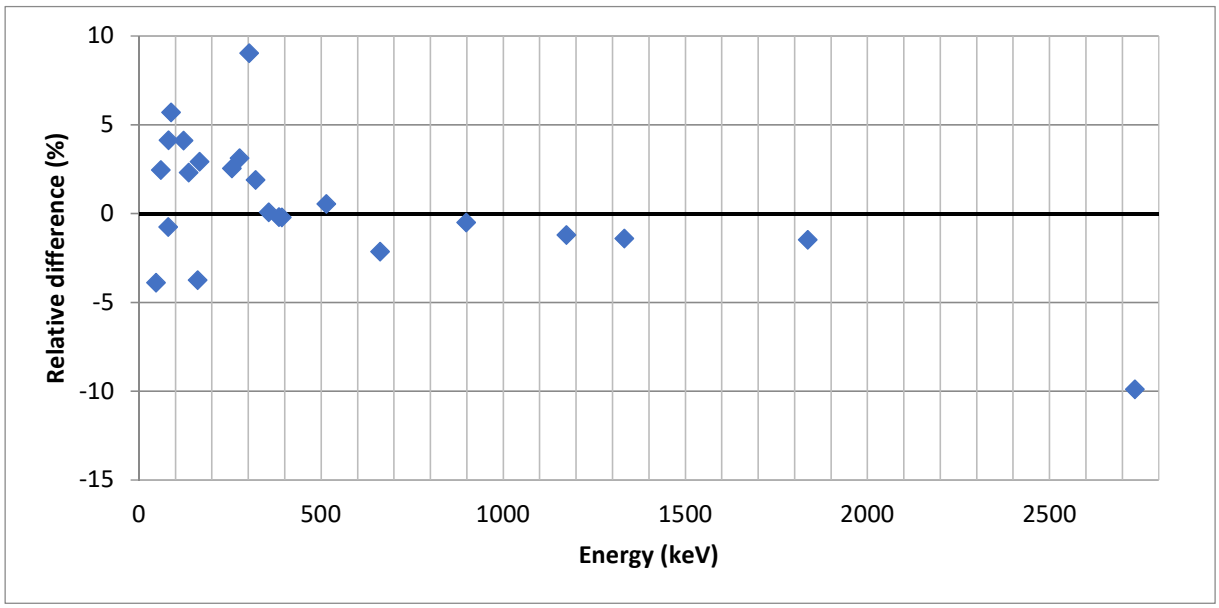

Figure 34: Relative difference ((experimental-simulation)/simulation)(for a volume source) of model 5 of detector T7

Model 6

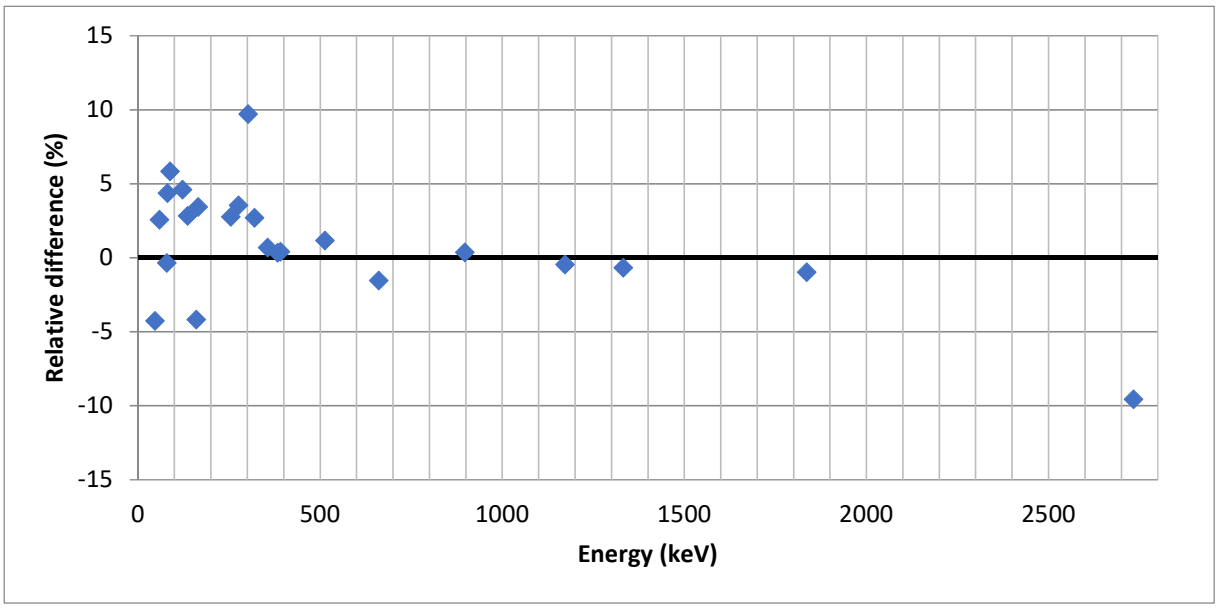

Figure 35: Relative difference ((experimental-simulation)/simulation)(for a volume source) of model 6 of detector T7

ANNEX B: counting efficiency calibration-curves for detector T2 and Ge-6

T2

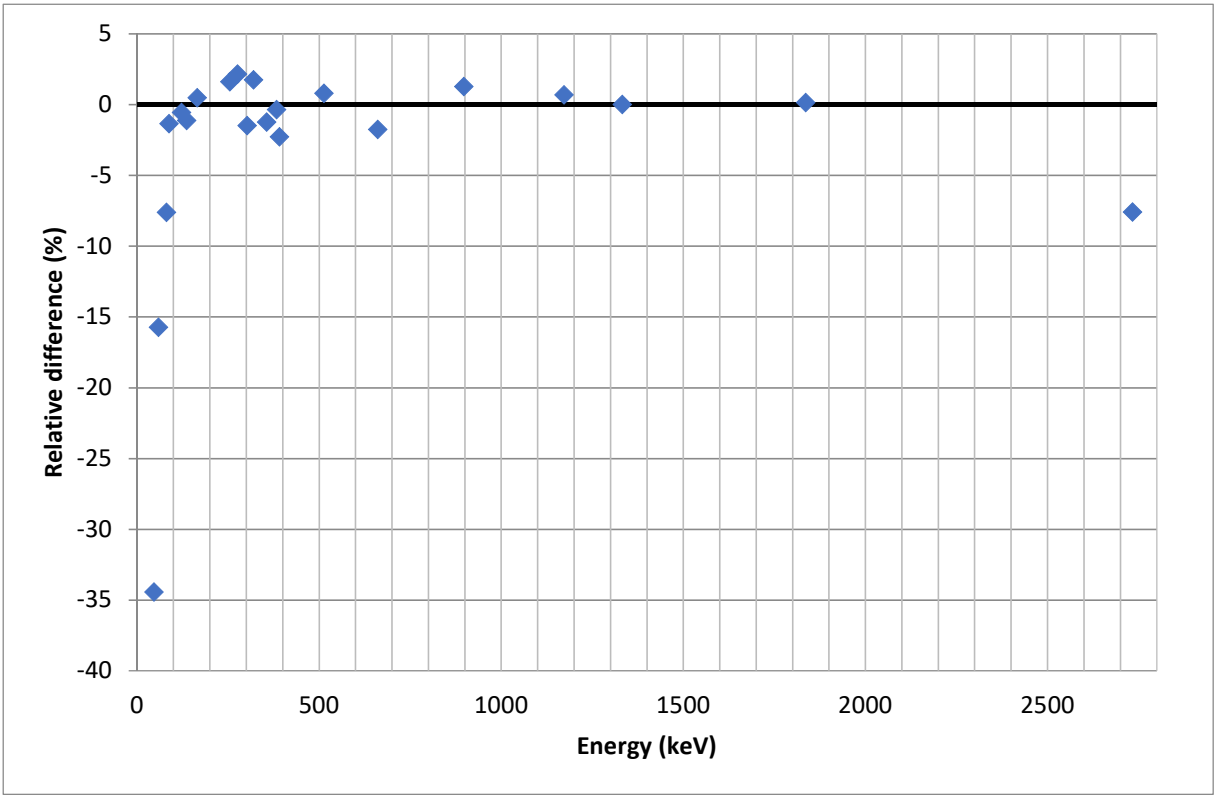

Figure 36: Relative difference ((experimental-simulation)/simulation)(for a volume source) of the model of T2 with a deadlayer thickness from the manufacturers datasheet

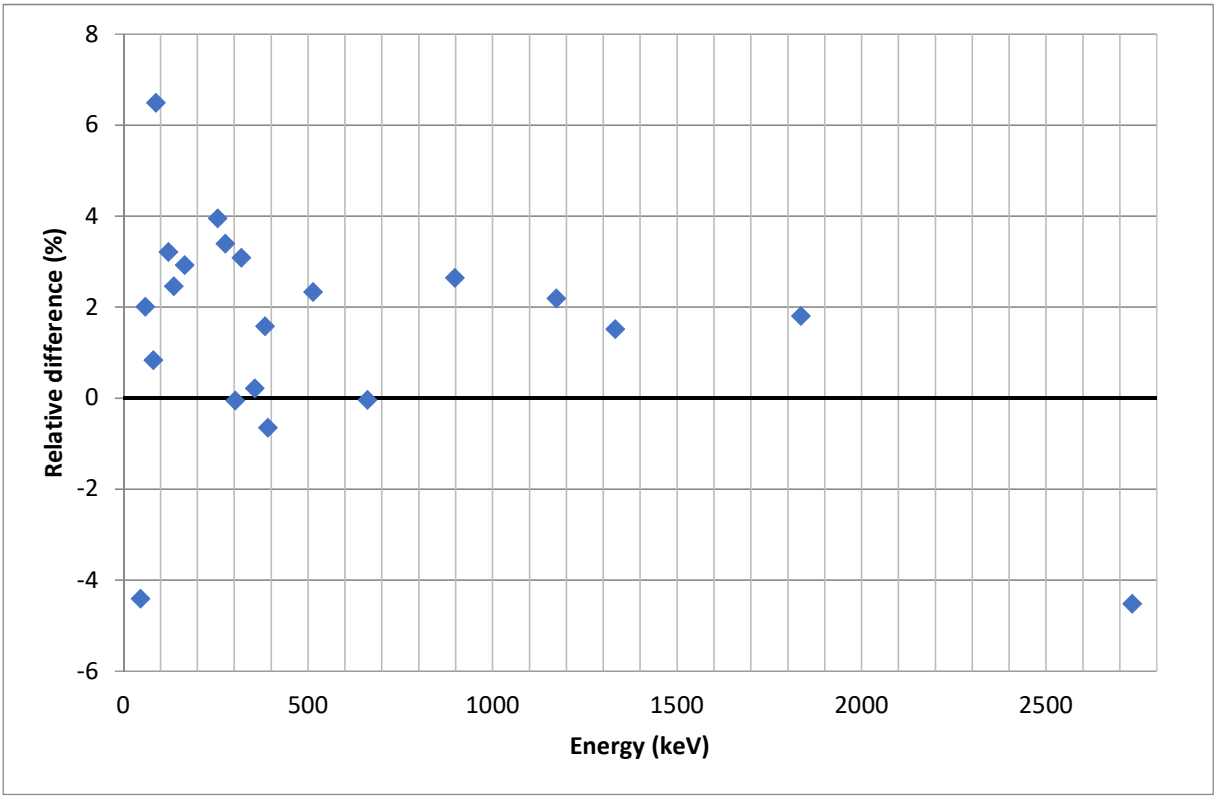

Figure 37: Relative difference ((experimental-simulation)/simulation)(for a volume source) of the model of T2 with a deadlayer thickness equal to the mean of the method from budjas et al. [1]

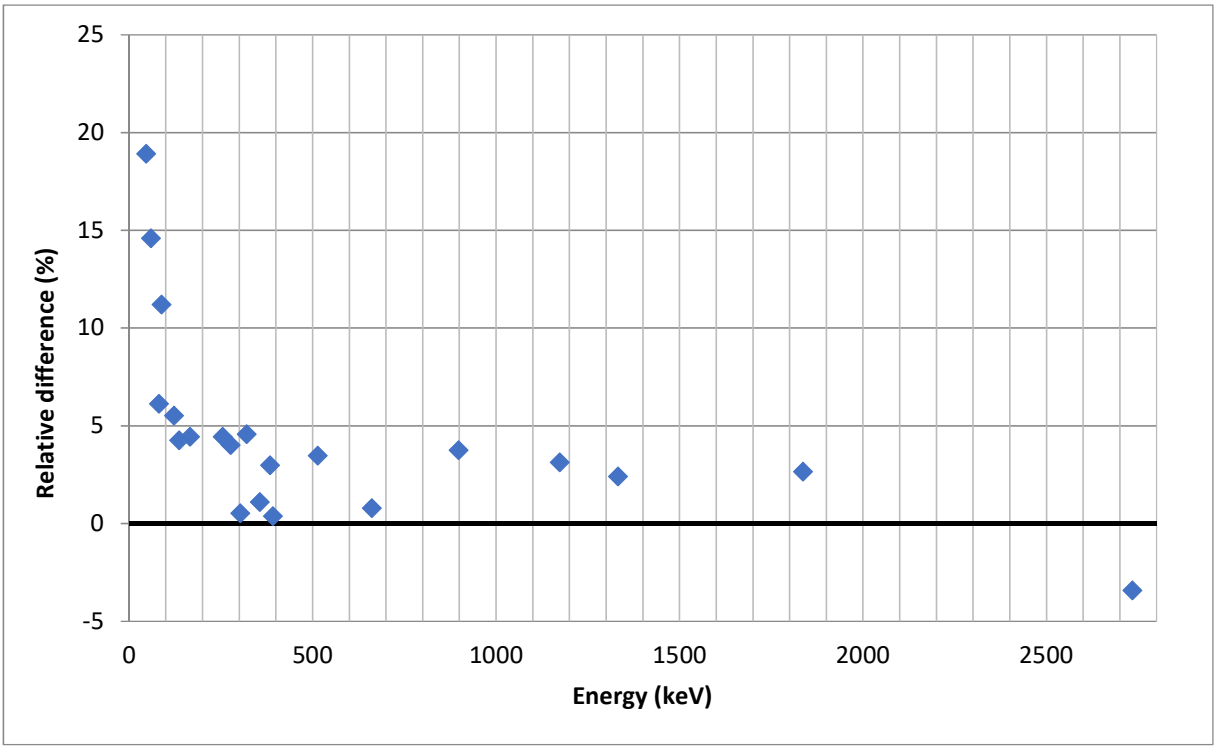

Figure 38: Relative difference ((experimental-simulation)/simulation)(for a volume source) of the model of T2 with a deadlayer thickness equal to the mean of the method based on the attenuation coefficients

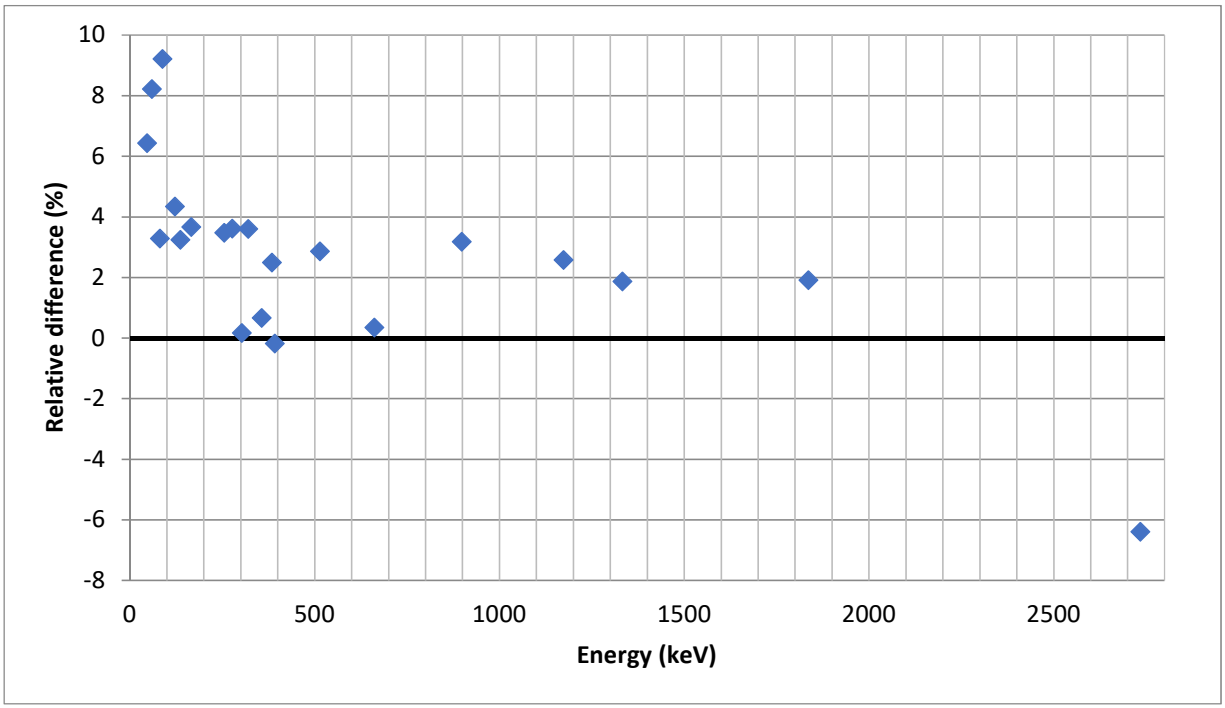

Figure 39: Relative difference ((experimental-simulation)/simulation)(for a volume source) of the model of T2 with a deadlayer thickness equal to the mean of the mean of both methods

Ge-6

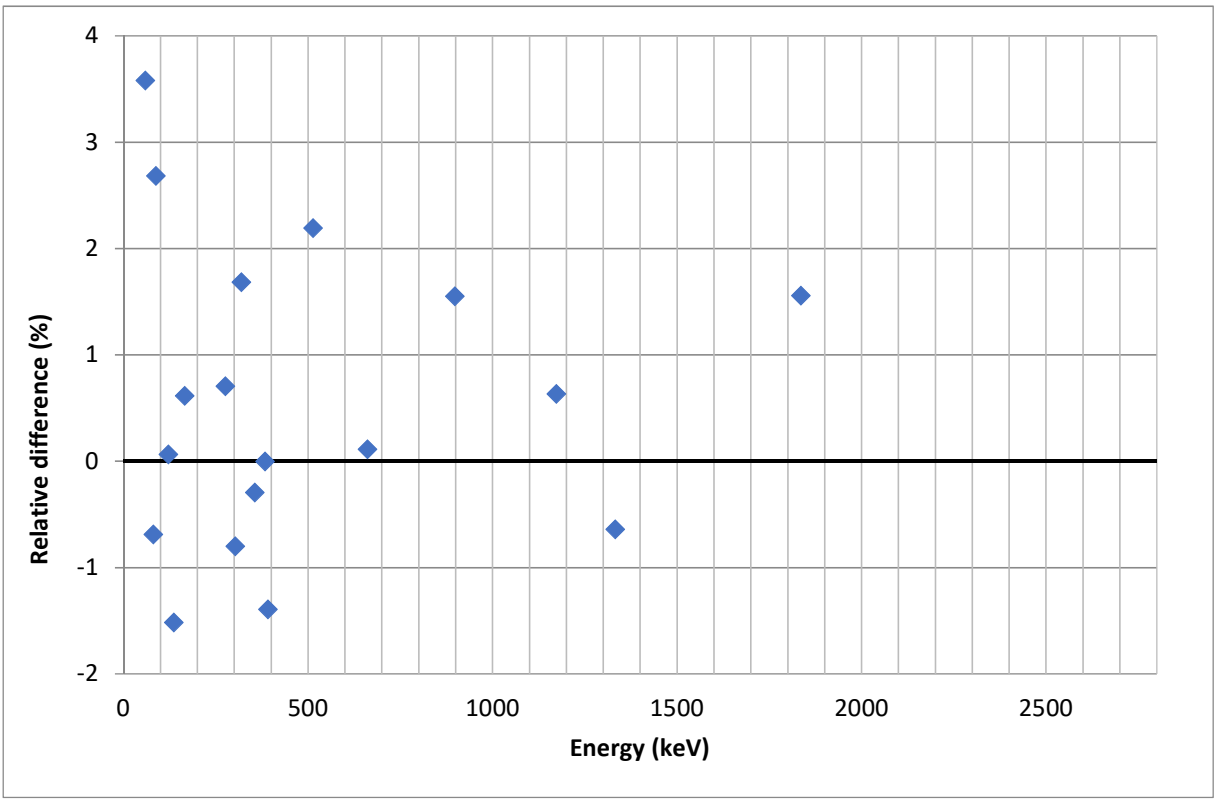

Figure 40: Relative difference ((experimental-simulation)/simulation)(for a volume source) of the model of Ge-6 with a deadlayer thickness of 1.50 mm

Auteursrechtelijke overeenkomst

Ik/wij verlenen het wereldwijde auteursrecht voor de ingediende eindverhandeling:
Study of parameters influencing the response of HPGe-detectors

Richting: **master in de industriële wetenschappen: nucleaire technologie-nucleaire technieken / medisch nucleaire technieken**
Jaar: **2018**

in alle mogelijke mediaformaten, - bestaande en in de toekomst te ontwikkelen - , aan de Universiteit Hasselt.

Niet tegenstaand deze toekenning van het auteursrecht aan de Universiteit Hasselt behoud ik als auteur het recht om de eindverhandeling, - in zijn geheel of gedeeltelijk -, vrij te reproduceren, (her)publiceren of distribueren zonder de toelating te moeten verkrijgen van de Universiteit Hasselt.

Ik bevestig dat de eindverhandeling mijn origineel werk is, en dat ik het recht heb om de rechten te verlenen die in deze overeenkomst worden beschreven. Ik verklaar tevens dat de eindverhandeling, naar mijn weten, het auteursrecht van anderen niet overtreedt.

Ik verklaar tevens dat ik voor het materiaal in de eindverhandeling dat beschermd wordt door het auteursrecht, de nodige toelatingen heb verkregen zodat ik deze ook aan de Universiteit Hasselt kan overdragen en dat dit duidelijk in de tekst en inhoud van de eindverhandeling werd genotificeerd.

Universiteit Hasselt zal mij als auteur(s) van de eindverhandeling identificeren en zal geen wijzigingen aanbrengen aan de eindverhandeling, uitgezonderd deze toegelaten door deze overeenkomst.

Voor akkoord,

Geelen, Stef

Datum: **4/06/2018**